Joint Centre for Mesoscale Meteorology, Reading, UK

Generation of near-surface gusts by deep convection

K. Nakamura
R. Kershaw

Internal Report No. 46

April 1995

Met Office Joint Centre for Mesoscale Meteorology Department of Meteorology
University of Reading PO Box 243 Reading RG6 6BB United Kingdom
Tel: +44 (0)118 931 8425 Fax: +44 (0)118 931 8791
www.metoffice.com

Designed and produced by the Met Office © Crown copyright 2001 01/0240 The Met Office logo is a registered trademark.

Generation of near-surface gusts by deep convection

Kozo Nakamura and Roy Kershaw

27th April 1995

Abstract

A parameterization of the production of near-surface gusts by convection is proposed for use in Numerical Weather Prediction models. A cloud-resolving model is used to investigate the phenomenon, and to validate the parameterization in a range of convective regimes, including two types of severe weather which affect the UK: mid-latitude depressions and thunderstorms. Two processes are shown to be important: downward transport of air with higher momentum by downdraughts, and the deflection of these downdraughts as they approach the surface.

1. Introduction

Strong gustiness in horizontal winds near the surface is often associated with convection, and these convectively generated gusts can cause disruption, damage, and sometimes death. The gales which disrupted the Fastnet Yacht Race on 14 August 1979 (Bond et al., 1981), and the Burns Day Storm of 25 January 1990, in which 47 people died, (Blackall et al. (1990)) are examples associated with mid-latitude depressions, when convection occurs in the presence of strong geostrophic winds. Damaging winds also occur in association with thunderstorms, where the convective downdraughts cause sudden variations in wind speed and direction at low levels, posing a significant hazard to aircraft on take off or landing (Fujita and Caracena (1977) give an analysis of three such accidents and the phenomenon has been modelled by Proctor (1988), Knupp (1989), Straka and Anderson (1993), and Parsons and Weisman (1993)). The purpose of this paper is to propose and test a parameterization of convectively generated gusts for use in Numerical Weather Prediction (NWP) models.

Convectively generated gusts are quite different in character from those generated by shear-driven turbulence (Bradbury and Deaves (1994)). This has implications for wind engineers and weather forecasters, as discussed in Collier et al. (1994) and Bradbury et al. (1994). In particular, we must consider the mechanisms of convective gust generation when designing a parameterization for use in a forecast model. There are two processes by which convection can enhance gustiness, above the levels normally produced by shear-driven turbulence. The first is the production of horizontal momentum by pressure gradient forces, as convective downdraughts are blocked by the surface and distorted to spread out horizontally. The second is the downward transport of horizontal momentum by the convective downdraughts, in the presence of vertical shear. Existing forecasting methods are usually based on these processes.

The method used in the UK Met Office for calculating peak gusts caused by thunderstorm downdraughts (Forecasters' Reference Book (1993)) is based on the relationship

found by Fawbush and Miller (1954) between the peak wind speed at the surface and the temperature drop associated with the downdraught. This effectively relates the strength of the gust to the negative buoyancy force in the downdraughts; it is thus based mainly on the first process, the conversion of downdraught kinetic energy to transverse kinetic energy. Being an empirical method, it may implicitly incorporate some element of the second process, vertical momentum transport, because vertical shear will have been present in most, if not all, of the severe thunderstorms which provided the data from which the relationship was deduced. Automating this method of gust prediction is one of the motivations of this paper.

In mid-latitude depressions, the gust speed can often be related to the wind speed at some upper level. Bond et al. (1981) showed that the speed of travel of radar echoes gave a good indication of the peak surface gusts at exposed coastal locations on several occasions of strong wind, including the Fastnet gale. The echo speed was characteristic of the wind speed one or two kilometres above the surface, suggesting that the momentum at those levels had been transported to the surface by downdraughts. In these cases, the shallow nature of the convection prevented vigorous downdraught development which might have generated gusts greatly in excess of the echo velocity. In these situations, and in the Burns Day storm (Blackall et al. (1990)), it seems likely that the gusts were produced primarily by momentum transport. When such storms occur, forecasters in the Central Forecasting Office at Bracknell tend to use the predicted winds at around 600m above ground level (AGL), from an NWP model, as a first estimate of the maximum gusts which are likely to occur at 10m AGL, the standard anemometer height (Bradbury et al. (1994)). We seek to improve on this estimate by developing a physically based parameterization scheme.

Such a scheme must work in both of the weather situations described above: thunderstorms and convection in mid-latitude depressions. Clearly, there will also be occasions when the two processes of convective gust generation are comparable in magnitude. Therefore, both processes must be included in the parameterization. We use a simple energy conservation argument to achieve this. We assume that an air parcel in a downdraught conserves its initial (horizontal) kinetic energy and that the work done by buoyancy forces generates additional horizontal kinetic energy. This gives us an equation for the maximum possible convective gust.

$$V_{gust} = \sqrt{\int_0^H -2g\left(\frac{\Delta\theta}{\Theta} - q_r\right) dz + v_{ini}(H)^2}$$

The remainder of this paper is devoted to testing the applicability of this equation in a range of conditions using a cloud-resolving model. We ran a series of numerical experiments to investigate the relative importance of the two gust generation processes in cases of varying vertical shear, varying geostrophic wind, and a recent thunderstorm case.

2. Model and initial condition

The model used is the Met. Office cloud-resolving model, which is described by Shutts and Gray (1994). It is a 3-dimensional anelastic model on a cartesian grid. The model includes prognostic equations for the three velocity components, liquid water temperature,

run	wind ($m\,s^{-1}$)				Coriolis	Geostrophic	
	$t=0min$		$t=30min$		parameter	wind($m\,s^{-1}$)	
	$z=0.05km$	$6km$	$z=0.05km$	$6km$	(s^{-1})	$z=0.05km$	$6km$
1	(0,0)	(0,0)	(0,0)	(0,0)	0	(0,0)	(0,0)
2	(0,0.19)	(0,20)	(0,2.1)	(0,19.5)	0	(0,0)	(0,0)
3	(0,0.38)	(0,40)	(0,4.2)	(0,38.9)	0	(0,0)	(0,0)
11	(0,0)	(0, 0)	(0,0)	(0,0)	10^{-4}	(0,0)	(0,0)
12	(0,10)	(0,10)	(–0.1, 8.7)	(0,10)	10^{-4}	(0,10)	(0,10)
13	(0,20)	(0,20)	(–0.2,16.4)	(0,20)	10^{-4}	(0,20)	(0,20)
14	(0,40)	(0,40)	(–0.6,29.9)	(0,40)	10^{-4}	(0,40)	(0,40)
21	(–10,–9.81)	(–10,10)	(–8.1,-7.0)	(–10.0,10.0)	10^{-4}	(–10,–9.81)	(–10,10)
22	(–10,0.19)	(–10,20)	(–8.5, 1.4)	(–10.0,20.0)	10^{-4}	(–10,0.19)	(–10,20)
23	(0,0.19)	(0,20)	(0.2,1.6)	(0.0,20.0)	10^{-4}	(0,0.19)	(0,20)
24	(10,0.19)	(10,20)	(8.8,1.6)	(10.0,20.0)	10^{-4}	(10,0.19)	(10,20)
31	(–7.5,5.2)	(4.9,15.3)	(–6.0,6.3)	(4.9,15.3)	0	(0,0)	(0,0)

Table 1 A summary of the initial wind fields and the geostrophic wind fields.

total moisture mixing ratio, and rain water content. A TVD advection scheme, which is positivity preserving, and a first order turbulence closure scheme, in which eddy viscosity and diffusivity are determined diagnostically from the local Richardson number, are used.

We performed four series of experiments. A summary of the initial conditions is shown in Table 1. In the first series, consisting of Runs 1, 2 and 3, the initial wind is zero or increases linearly with height to $z = 6km$; we investigate the production of convective gusts in the presence of linear unidirectional shear. In the second series, consisting of Run 11 to Run 14, the initial wind is geostrophic, in order to simulate gust production in varying geostrophic winds. In the third series, consisting of Run 21 to Run 24, we simulate gust production in directional shear. The last experiment (31) simulates a thunderstorm on 24th of June 1994, when gusts of up to 27 $m\,s^{-1}$ were observed over South Eastern England.

The first three series use a small computational domain, $50km \times 50km \times 15km$, while the last experiment uses a larger computational domain, $250km \times 250km \times 15km$. The horizontal grid spacings are $dx = dy = 1km$ and $dx = dy = 2.5km$, respectively. In all experiments, there are 30 variably spaced levels in the vertical with 10 levels in the lowest $1.5km$ and the smallest vertical grid spacing is about $100m$. Cyclic lateral boundary conditions are used, and there is a damping layer at the top of the domain above $z=10km$.

The initial fields are horizontally uniform. Fig. 1 shows the vertical profiles of temperature and dew point temperature which were used as initial conditions for Runs 1-24. The temperature lapse rate is neutral to dry ascent below $z = 1.5km$, neutral to moist ascent around $z=2km$, and absolutely stable above $z=3km$. The relative humidity is 80 % below $z=2km$ level, and it decreases linearly to 0 % at the top of the computational domain. The vertical profiles of temperature, dew point temperature, and wind velocity and direction used in Run 31 will be shown later in Fig. 19.

In Runs 1-24, we add small random initial disturbances of potential temperature at the lowest level, and constant heat and moisture fluxes at the surface (100 $W\ m^{-2}$ sensible heat flux and 1200 $W\ m^{-2}$ latent heat flux). In the runs with non-zero Coriolis force, the heat fluxes are set to zero during the first 30 minutes so that the wind profile in the

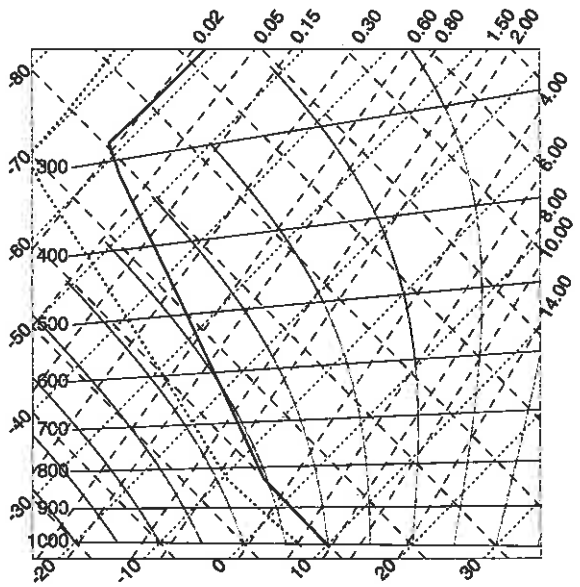

Figure 1: Vertical profiles of initial temperature and dew point temperature for Run 1 – Run 24 on a tephigram. The thick solid line indicates temperature, and the thick dashed line indicates dew point temperature.

boundary layer adjusts to surface friction, as in a neutral Ekman layer.

In Run 31, a thermal bubble of radius $10km$ and height $3km$ is used as the initial disturbance in order to restrict the region of occurrence of active convection. The surface fluxes of sensible and latent heat are both set to 200 $W\ m^{-2}$ during the first 30 minutes and then reduced to 10 $W\ m^{-2}$ after $t{=}30min$. Each experiment is run for more than 4 hours.

3. Results without Coriolis force

3.1. Run 1 with neither basic wind nor Coriolis force

Lots of convection cells developed at first because of the random initial disturbances. The depth and width of the cells became larger and larger with time. Clouds formed at about $t = 30min$, when convection became more active. Fig. 2 shows time series of (a) the maximum speeds of up and downdraughts, (b) the maximum surface gust, i.e., the maximum horizontal wind speed at the lowest grid level, and (c) the maximum rain water mixing ratio and the maximum negative deviation of temperature from the horizontal average. The maximum gust speed of 9.7 $m\,s^{-1}$ occurred at $t = 285min$, while many other maximum values occurred because many convective cells developed and dissipated successively at various positions. The time series show in general that large negative buoyancy force and rain water content were produced in association with active upward motions, and that the occurrence of large water content in the upper layer was followed by large water content near the surface, which was followed by a gust at the surface. We can find a lot of occurrences of large gust speeds in the time series. We will use the six peak values at $t = 98, 134, 168, 250, 272$ and $285min$ in order to validate a parameterization equation to estimate the gust speed later in section 3.3, while we will discuss the peak

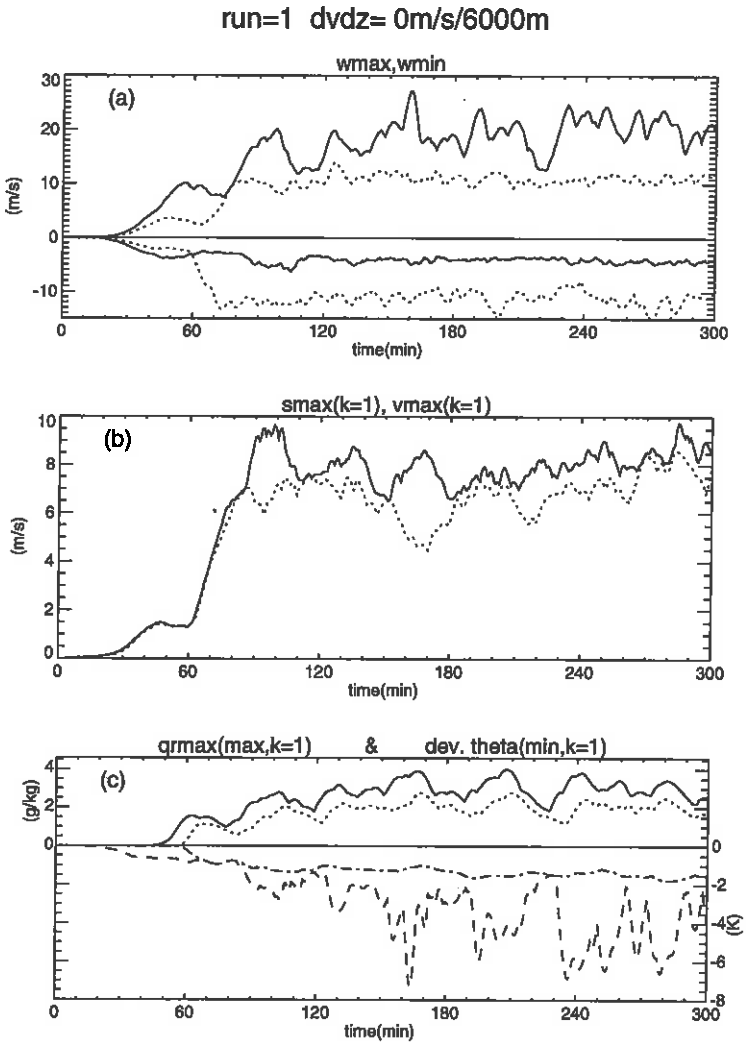

Figure 2: Time series of (a) the maximum updraughts and downdraughts, (b) the maximum surface gust, i.e., the maximum horizontal wind speed (solid line), and maximum v velocity (dotted line) at the lowest grid level, and (c) the maximum rain water mixing ratio and the maximum negative deviation of temperature from the horizontal average. The solid lines in (a) and (c) and dashed line in (c) indicate the maximum values in the whole domain, while the dotted lines and dash-dotted line indicate the maximum values in the lowest grid level, i.e., $z=0.1km$ for w and $z=0.06km$ for others. The values of w at $z=0.1km$ are multiplied by 10.

gust at $t=285min$ in this section.

The horizontal cross section at the lowest level at $t=284min$, 1 minute before the gust attained the maximum speed, is shown in Fig. 3a. The maximum horizontal wind speed at the lowest level of $9.7\,m\,s^{-1}$ occurred at ($x=11km$, $y=12km$), where the air spread out from the downdraught centred at ($x=10km$, $y=10km$) to form a gust front marked by the surrounding updraught. Thus, the downdraught hit the surface and produced the horizontal gust. Note that the updraughts at this level have a varicose structure.

The maximum upward motion at this moment was $16.3\,m\,s^{-1}$ which occurred at ($x=10km$, $y=10km$, $z=6.6km$) in the same convective cell making the maximum gust at the surface. In this region there is a downdraught in the lower levels (Fig. 3b). The maximum

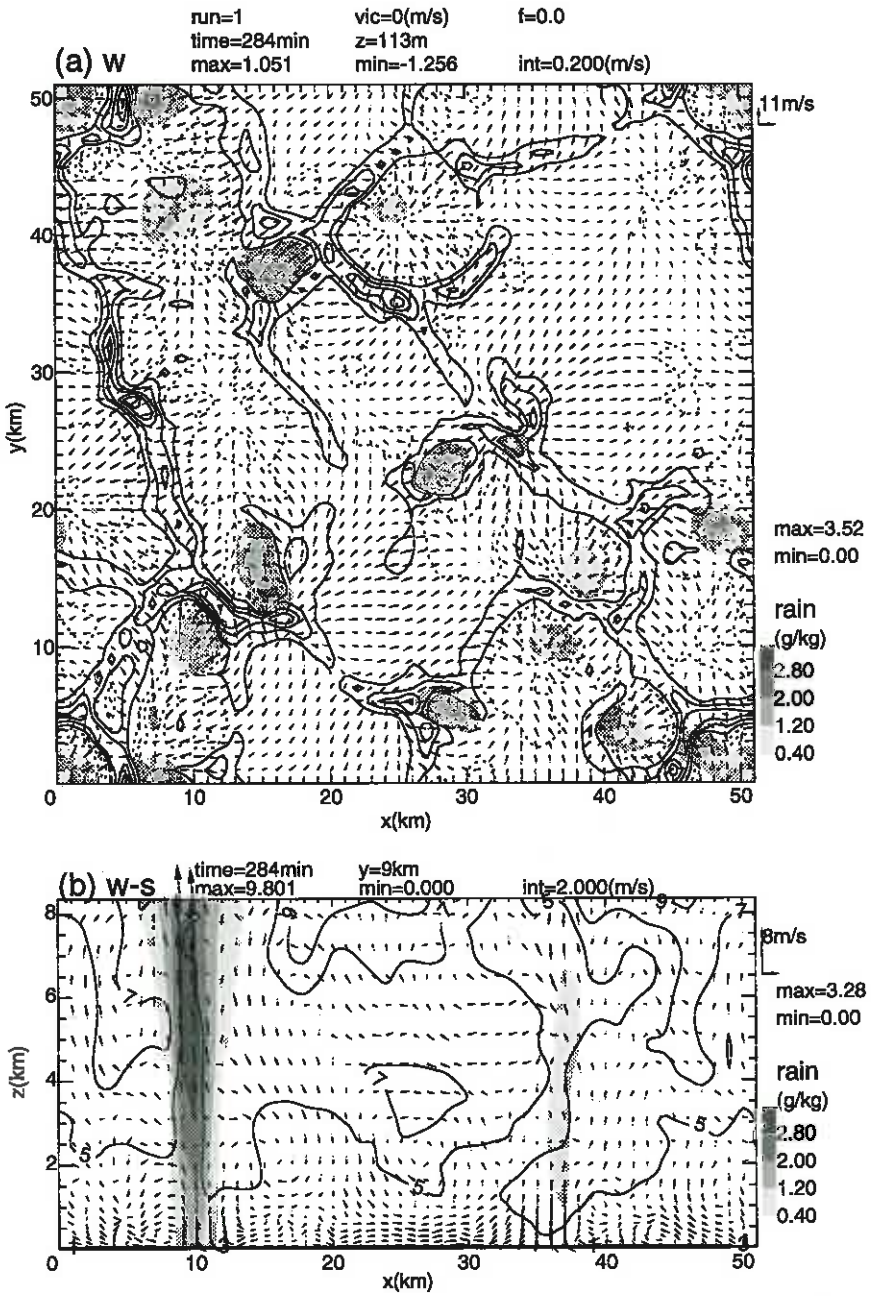

Figure 3: (a) Horizontal cross section of horizontal winds, vertical velocity, and rain water mixing ratio at the lowest level at $t = 284min$, 1 minute before the gust attained the maximum speed in Run 1. Arrows indicate horizontal velocity, (u, v). Solid and dashed lines indicate contours of w. The contour interval is $0.2\,m\,s^{-1}$, and the solid lines indicate the contours of $0.1, 0.3, 0.5, \ldots m\,s^{-1}$ and dotted lines $-0.1, -0.3, \ldots m\,s^{-1}$. The shaded areas define the region with rain water mixing ratio more than $0.4\,g\,kg^{-1}$. (b) x-z vertical cross section through the maximum surface gust. The arrows indicate (u, w) velocity. The solid lines indicate contours of horizontal wind speed. The shaded areas contain rain water mixing ratio more than $0.4\,g\,kg^{-1}$.

speed of the downdraught was $-2.6\,m\,s^{-1}$ at $(x = 11km,\ y = 10km,\ z = 0.6km)$. The air in the upper level updraught in this region was supplied not from below but from the surrounding area. The updraught inflow was cut off and the convection dissipated when the gust spread and prohibited upward motion in the surrounding area.

The time changes of w, rain water content, potential temperature deviation, and horizontal wind-speed at the lowest level for $x = 10km$ are shown in Fig. 4. Several convective cells started to develop about $t = 30min$. After the development of the first convection, downdraughts occurred with rain by $t = 60min$ and the next updraughts developed between the downdraughts, where the spreadings from adjacent cells collided to produce updraughts. Some of them were more active and produced more rain and stronger downdraughts and horizontal winds. The strongest horizontal winds are usually located at the boundary between upward and downward motions, which is coincident with the boundary of the cold downdraught air as shown in Fig. 4b. The convection which made the maximum wind speed at $t = 285min$ started to develop about $t = 240min$. The maximum wind speed increased with time, moving in the positive y-direction from $y = 5km$ at $t = 265min$ to $y = 11km$ at $t = 285min$. The time scale of the convection, i.e., the time from the beginning of the updraught to the end of the rain was about $t = 60min$, which is in agreement with the results of many investigations of isolated convection.

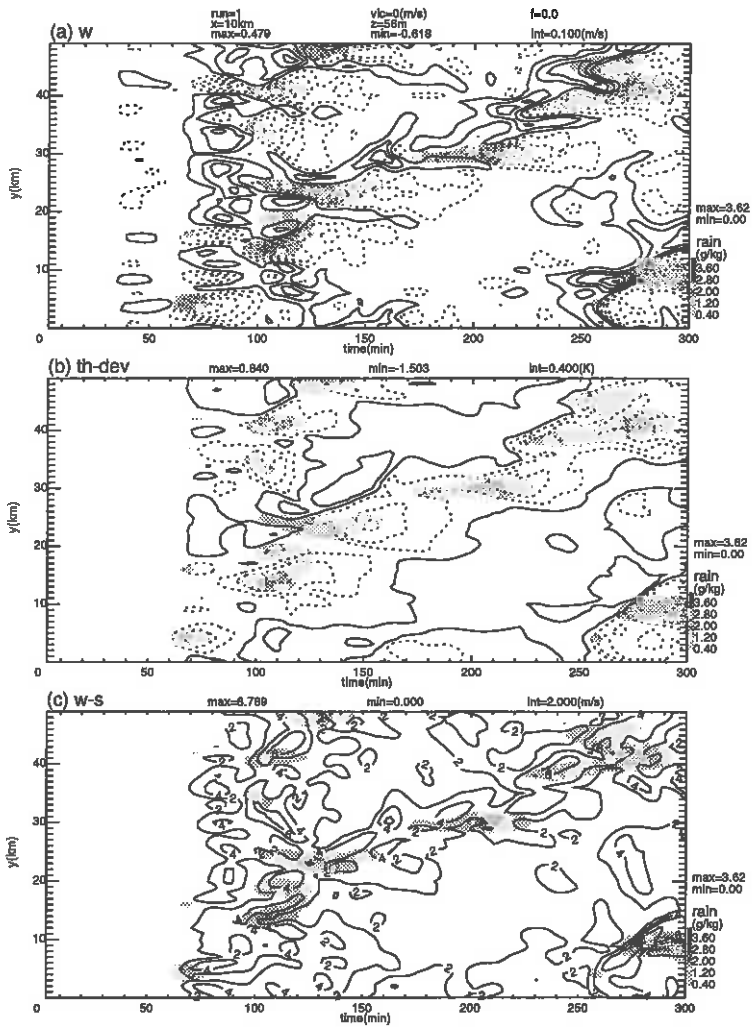

Figure 4: y-t diagrams for the line $x = 10km$ at the lowest grid level for Run 1, (a) w, (b) potential temperature deviation from the horizontal average and (c) horizontal wind speed. The shaded areas indicate rain water mixing ratio more than $0.4\, g\, kg^{-1}$.

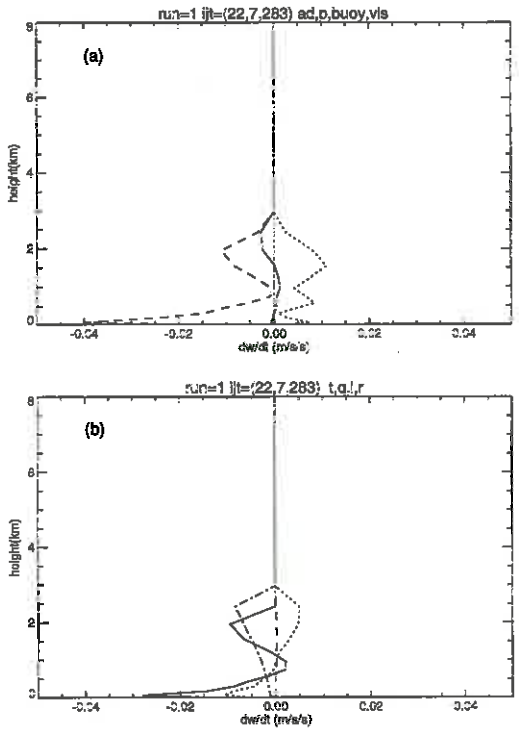

Figure 5: (a) Vertical profiles of each term of equation (2) in the downdraught at $x=10km$, $y=8km$ and $t=283min$. The solid line indicates the advection term, dotted line the pressure gradient term, dashed line the buoyancy term, and dash-dotted line the viscosity term. Data are only plotted below $z=3km$ because the downdraught started there. (b) Vertical profiles of each term of equation (3) at the same time and position as (a). The solid line indicates the temperature deviation term, dotted line the water vapour term, dashed line the cloud water term, and dash-dotted line the rain water term.

The maximum gust speed produced by such convection can be estimated by considering the energetics of the downdraughts. The anelastic momentum equation can be written as

$$\frac{d\vec{v}}{dt} = \frac{\partial \vec{v}}{\partial t} + \vec{v} \cdot \nabla \vec{v} = -\nabla \left(\frac{p'}{\rho_s} \right) + B\vec{k} + \overrightarrow{Vis} \tag{1}$$

where $\vec{v}$ is the vector velocity (u, v, w) in (x, y, z) coordinates, ρ_s the reference density at each level, p' the perturbation pressure, B the buoyancy term, and $\overrightarrow{Vis}$ the turbulent term due to subgrid scale motions. The vertical component of equation (1) is written as

$$\frac{dw}{dt} = \frac{\partial w}{\partial t} + \vec{v} \cdot \nabla w = -\frac{\partial}{\partial z} \left(\frac{p'}{\rho_s} \right) + B + \overrightarrow{Vis}_z. \tag{2}$$

where $\overrightarrow{Vis}_z$ is the vertical component of the turbulent term.

A typical example of the vertical profile of each term of equation (2) in the downdraught is shown in Fig. 5a. The primary term driving the downward acceleration is the buoyancy term, B, which is opposed by the upward directed pressure gradient term. The buoyancy term can be written as

$$B = g(\frac{\Delta\theta}{\Theta} + a\,\Delta q_v - \Delta q_c - \Delta q_r) \tag{3}$$

where g is the acceleration due to gravity, Δ indicates the deviation from the horizontal average, θ the potential temperature, Θ the reference potential temperature at each level, a a coefficient for buoyancy from the ratio between dry air and water gas constants, q_v, q_c, and q_r are the rain mixing ratios of water vapour, cloud water and rain water, respectively. Fig. 5b shows the vertical profile of each term of equation (3). The main terms driving the downdraught are the negative temperature deviation and the rain loading. The former was large in the lower levels, where the evaporation of rain cooled the air below cloud base, while the latter is large in the middle levels. The maximum water content was 0.98 $g\,kg^{-1}$ at $z = 2.4km$, whose loading effect on the buoyancy corresponded to $-0.28K$ of temperature deviation and 0.0096 $m\,s^{-2}$ downward acceleration in the momentum equation. The minimum temperature deviation was –0.81K at $z = 0.05km$, which gave 0.028 $m\,s^{-2}$ acceleration and was larger than the effect of the rain water loading. The tendency for the downdraught to be driven by rain loading at first and then negative temperature agrees with the results of previous investigations such as Proctor (1988), Knupp (1989), and Parsons and Weisman (1993).

In order to evaluate the importance of these terms in producing the downdraught, we estimate their effects as follows. If we approximate the equation (2) by

$$\frac{dw}{dt} = g(\frac{\Delta\theta}{\Theta} - q_r), \tag{4}$$

because the horizontal average of q_r is very small and the effects of Δq_v and Δq_c are much smaller than the effect of Δq_r, and modify it to

$$\frac{dw}{dt} = \frac{dz}{dt}\frac{dw}{dz} = w\frac{dw}{dz} = \frac{1}{2}\frac{dw^2}{dz} = g(\frac{\Delta\theta}{\Theta} - q_r) \tag{5}$$

and integrate it from z=0 to H defined as the starting point of the downdraught, we obtain the equation for estimating w due to buoyancy force at z=0 as

$$w_{z=0}^{\downarrow B} = \sqrt{\int_0^H -2g\left(\frac{\Delta\theta}{\Theta} - q_r\right)dz}. \tag{6}$$

If we calculate each of the two terms in the integration separately, we obtain equations for w due to temperature deviation and due to rain loading, respectively, as

$$w_{z=0}^{\downarrow T} = \sqrt{\int_0^H 2g\left(\frac{-\Delta\theta}{\Theta}\right)dz}, \tag{7}$$

and

$$w_{z=0}^{\downarrow R} = \sqrt{\int_0^H 2g(q_r)dz}. \tag{8}$$

If we estimate the values of $w_{z=0}^{\downarrow T}$ and $w_{z=0}^{\downarrow R}$ from Fig. 5b , they are 3.60 $m\,s^{-1}$ and 3.89 $m\,s^{-1}$ respectively. Although the maximum value of the effect of the temperature deviation is larger than the rain loading effect, its integrated effect is smaller than the rain loading effect because of the positive temperature deviation in the upper region and the shallow depth of the region of negative temperature deviation. The maximum values of $w_{z=0}^{\downarrow T}$ and $w_{z=0}^{\downarrow R}$ in the region between $y = 0km$ and $y = 10km$ at $x = 10km$ during the period from $t = 270min$ to $t = 285min$ were 6.03 $m\,s^{-1}$ and 7.63 $m\,s^{-1}$, respectively. The magnitudes

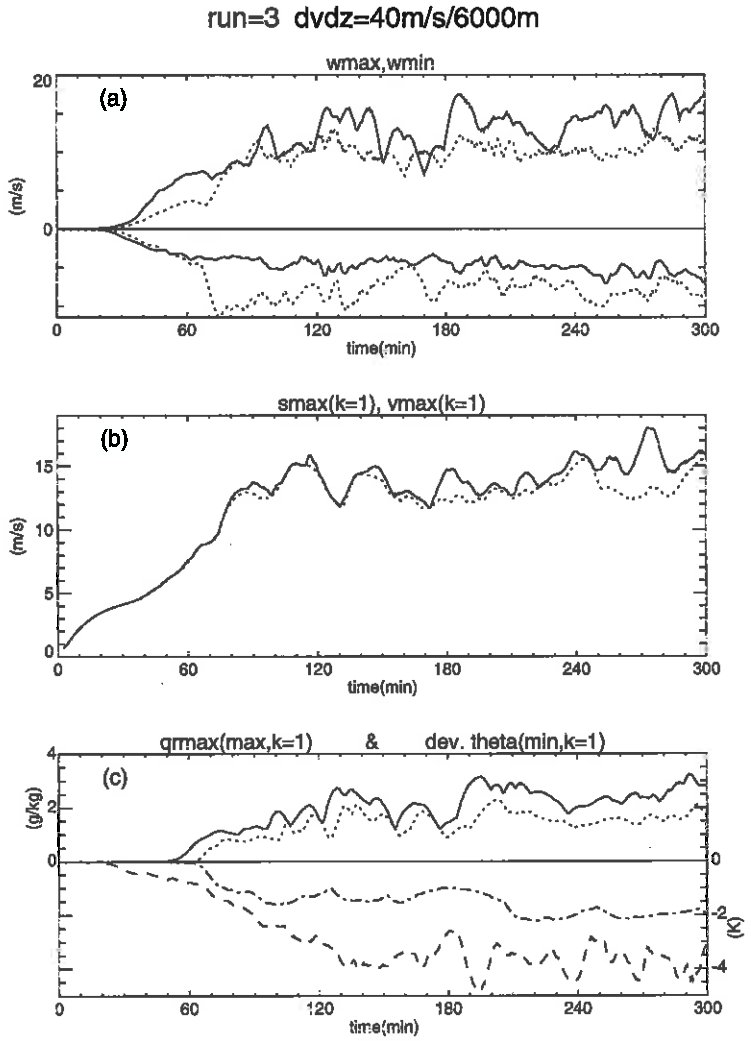

Figure 6: Time series of the peak values in Run 3 in the same format as in Fig. 2.

of the two terms are almost the same and both terms were important in producing the downdraught.

The speeds of the downdraughts decreased near the surface because of the upward directed pressure gradient force. If we assume that the work done by the buoyancy force is all used to produce horizontal velocity, i.e., the kinetic energy of the downdraught conserved in the turning at the surface, $w_{z=0}^{\downarrow B}$ must be a good estimate for the maximum horizontal gust. If we combine the two maximum values of $w_{z=0}^{\downarrow T}$ and $w_{z=0}^{\downarrow R}$ to get the peak value of $w_{z=0}^{\downarrow B}$, the value becomes $9.49\, m\, s^{-1}$ which is a good estimate of the gust speed realized in the experiment of $9.7\, m\, s^{-1}$.

3.2. Run 3 with basic wind shear and no Coriolis force

The time series of the peak values in Run 3 are shown in Fig. 6 in the same format as Fig. 2. The maximum gust speed at the lowest level was $18.0\, m\, s^{-1}$ and occurred at $t = 273 min$. The maximum updraught, temperature deviation and water content were a

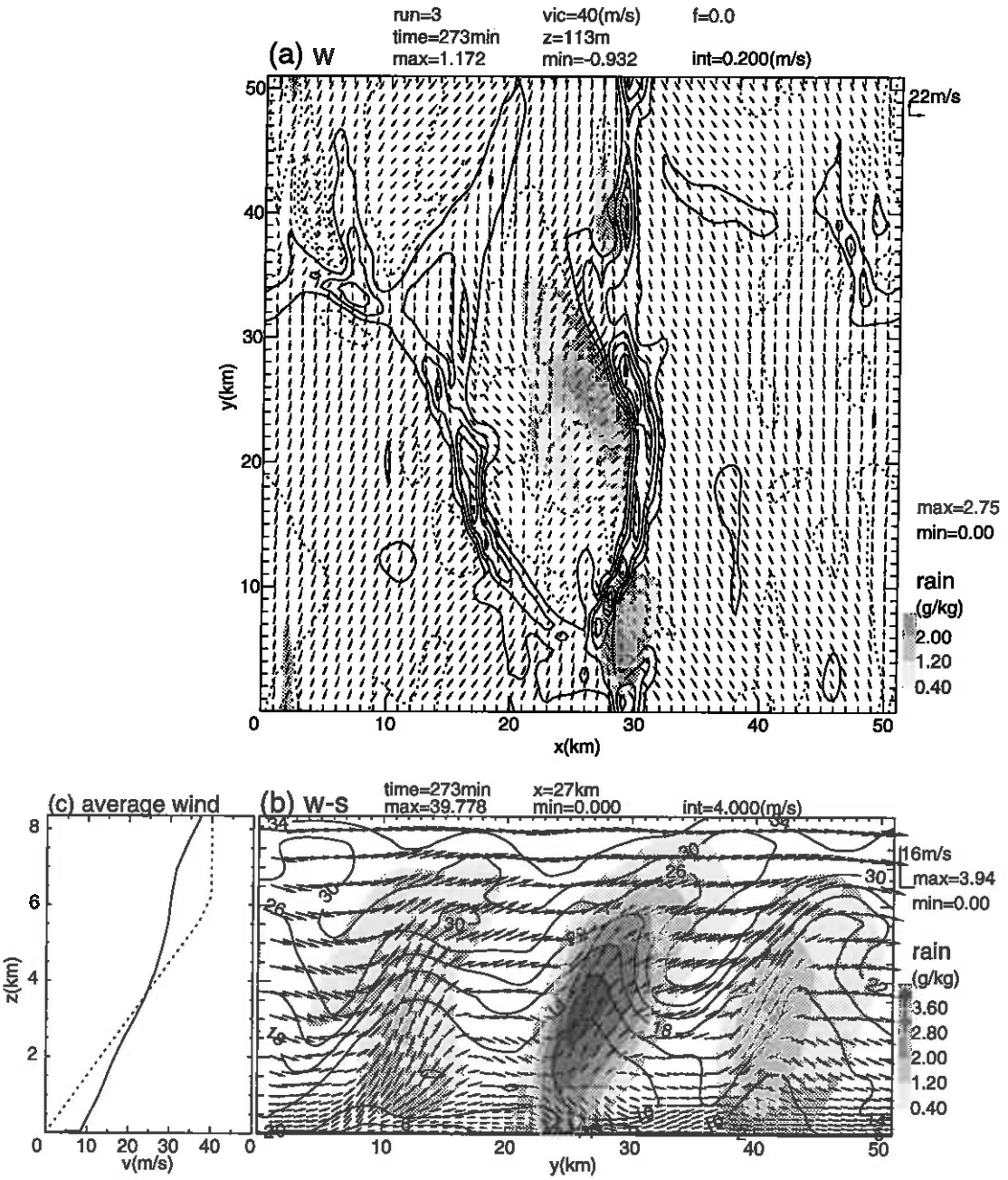

Figure 7: (a) Horizontal and (b) vertical cross sections as in Fig. 3 for Run 3 at $t=273min$, when the gust attained the maximum speed, (c) vertical profiles of average horizontal wind speed at $t=273min$ (solid line) and $t=0$ (dotted line), (d) horizontal wind velocity relative to the cloud movement at $z=2.2km$, and (e) vertical cross section through the maximum surface gust in the direction of the cloud movement. The arrows in (e) indicate the relative velocity in the vertical section and the solid and dotted lines indicate the contour lines of w.

little smaller than the results in Run 1. This is because convection was suppressed by the vertical shear in this run. However, the gust speed was much larger than in Run 1 because the initial momentum was transported to the surface in this run. We will use the six peak values at $t=89,116,146,182,239$ and $273min$ in order to validate a parameterization equation to estimate gust speeds later in section 3.3, while we will discuss the peak gust at $t=273min$ in this section.

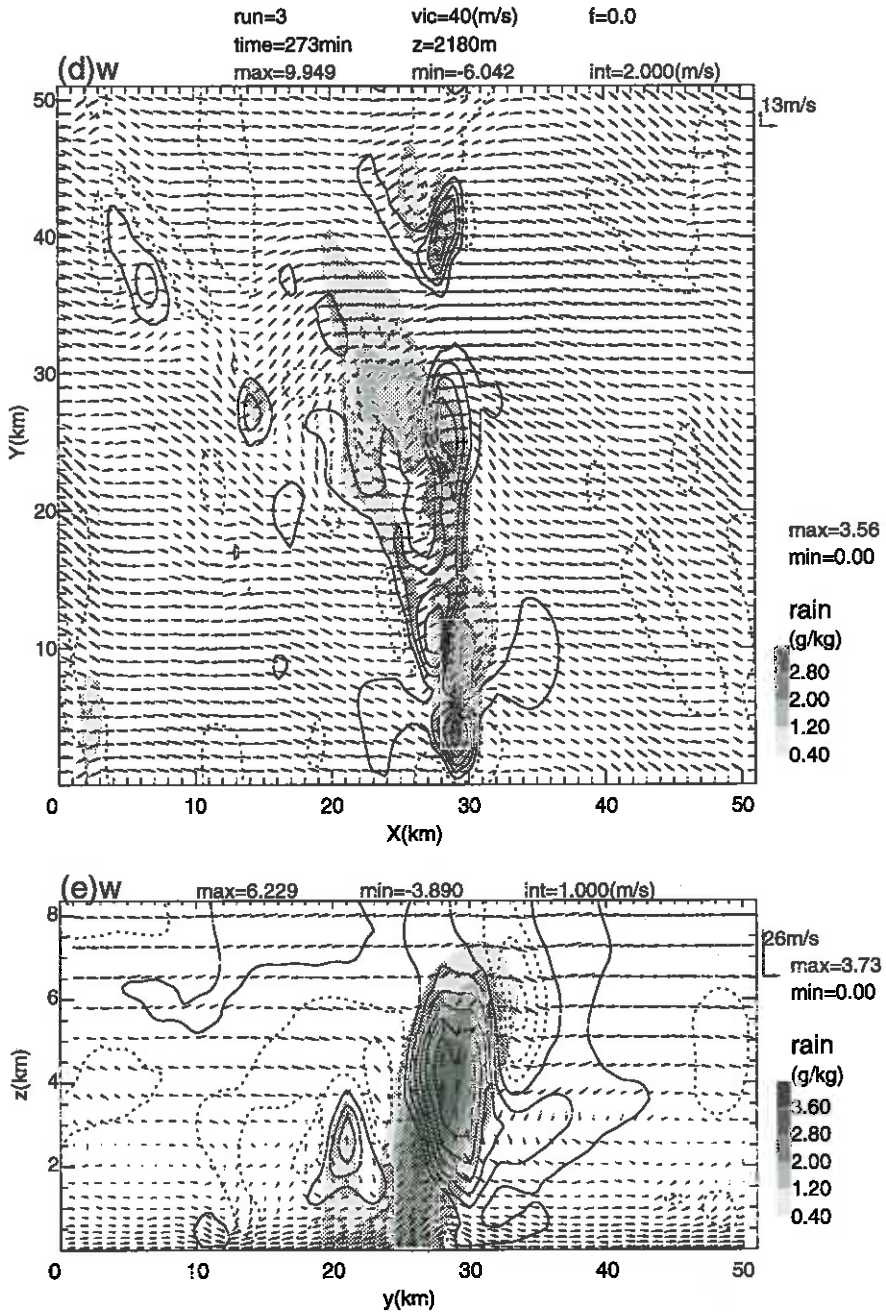

Figure 7: Continued.

Fig. 7a shows the horizontal cross section at the lowest level at $t = 273min$, when the gust attained the maximum speed. The maximum horizontal wind speed at the lowest level was 18.0 $m\,s^{-1}$ at ($x = 27km$, $y = 28km$) between the maximum upward motion at ($x = 29km$, $y = 27km$) and the maximum downward motion at ($x = 26km$, $y = 26km$). At first in this run many convective cells developed, but by this stage one large cell dominates the pattern. The upward motion which marks the gust front occurred in a shape of an oval surrounding the main rain area. The maximum velocity was located near the downwind position of the downdraught, where the air spread out in the same direction as the movement of the downdraught.

At the maximum gust point ($x = 27km$, $y = 28km$), there was an updraught above

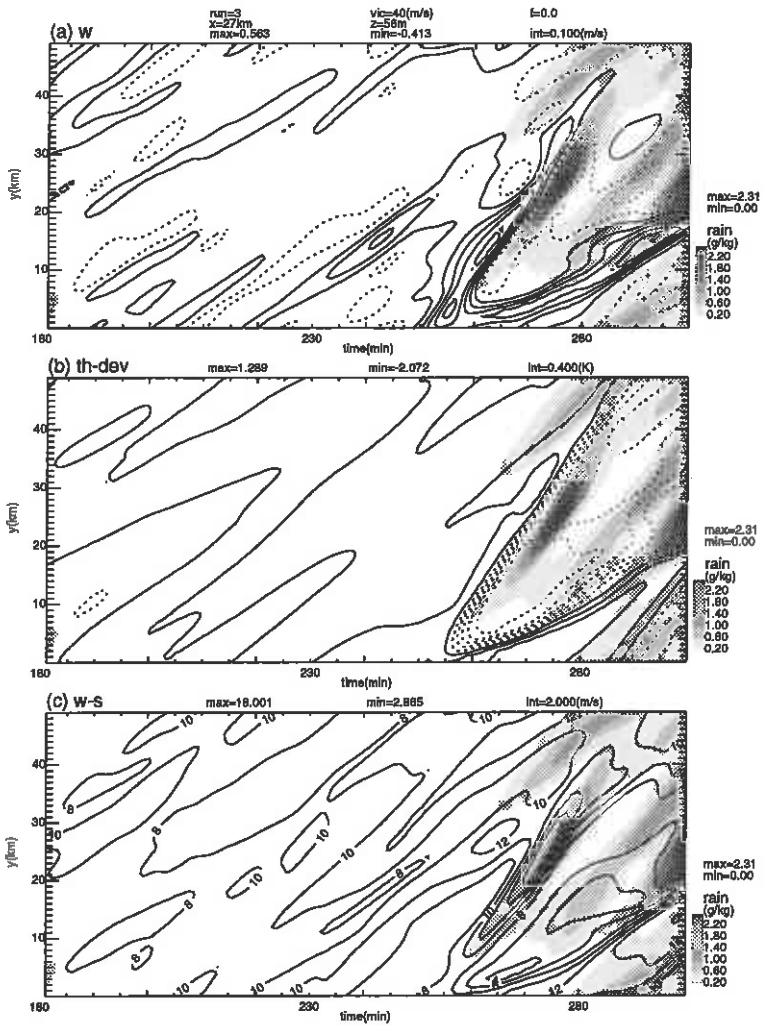

Figure 8: y-t diagrams for the line $x = 26km$ at the lowest grid level for Run 3, (a) w, (b) potential temperature deviation from the horizontal average and (c) horizontal wind speed in the same format as in Fig. 4. The shaded areas indicate rain water mixing ratio more than $0.4\,g\,kg^{-1}$.

$z = 1.75km$ and downdraught below that level (Fig. 7b). All the region below $z = 6km$ contained more than $0.4\,g\,kg^{-1}$ rain of water. This suggests the important role of rain loading in producing the downdraught as in the case of Fig. 3b. In general, as is shown in Fig. 7c, the horizontal wind was large in the upper region because of the initial conditions though the convection has reduced the shear. The upward motion transported lower momentum air upwards, whilst the compensating downward motion in the mid-troposphere has transported higher momentum air downwards. Note, however, that the horizontal wind has a peak value at the lowest grid level around $y = 28km$ and a minimum value around $z = 1km$ (Fig. 7b).

The propagation speed of the cloud producing the maximum gust was about ($u_{cloud} = 6.6\,m\,s^{-1}$, $v_{cloud} = 15.2\,m\,s^{-1}$) which was evaluated from the movement of the positions of the maximum upward and downward velocity at the lowest level from $t = 270min$ to $t = 280min$. The horizontal wind pattern relative to the cloud movement at $z = 2.2km$ in Fig. 7d shows the horizontal flow which passes around the right side of the updraught

and feeds into the downdraught located on the left side of the updraught. On the other hand the vertical cross section in the direction of the cloud movement in Fig. 7e shows the upshear tilt of the updraught. The rain produced in the updraught precipitated behind the updraught to produce downdraught and the convergence between the downdraught and the lower environmental wind enhanced the updraught in front of the cloud. The features are similar to the conceptual model of Browning (1964) and the results of numerical experiments of Klemp and Wilhelmson (1978) for the right moving super cell storms. The convection cell lasted longer than the one in Run 1 because the downdraught did not cut off the inflow near the surface.

The time changes of w, rain water content, potential temperature deviation, and horizontal wind-speed at the lowest level for $x=27km$ are shown in Fig. 8. The patterns show that the updraught region in the line structure related to the maximum gust moved in the y-direction at the speed of about $24\,m\,s^{-1}$, which is different from the cloud movement (u_{cloud}, v_{cloud}) because of the line structure and the inclination between the line and the x-axis. The spreading out of the downdraught from the convection center is shown clearly by the cold air region in Fig. 8b. It is important to note that the region of the maximum wind speed was located in the larger-y side of the rain region which corresponded to the region between the large downward motion and the large upward motion. It is also important to note that the wind speed grew with time moving in the y-direction. The growth of the wind speed could not be attained by advection because the wind speed was larger at $x=27km$ than $x=26km$ as is shown in Fig. 7a, and the wind speed is larger at the lowest grid level than the wind above as is shown in Fig. 7b.

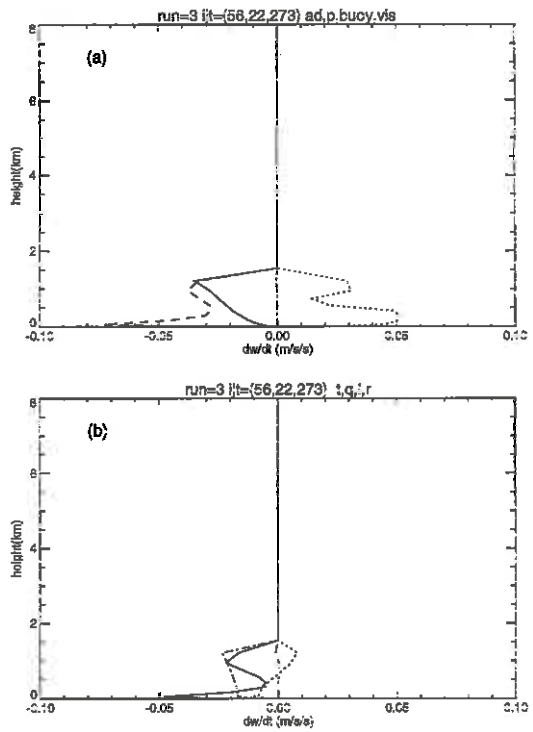

Figure 9: Vertical profiles of each term of equations (2) and (3) in the downdraught at $x=27km$, $y=22km$ and $t=283min$ for Run 3 in the same format as in Fig. 5.

The vertical profiles of each term of equations (2) and (3) in the downdraught at ($x = 27km$, $y = 22km$) at $t = 273min$ are shown in Fig. 9. The main terms driving the downward acceleration are advection terms and buoyancy terms due to negative temperature deviation and rain loading. The maximum water content was $2.54g\ kg^{-1}$ at $z = 1.2km$, so the loading effect on the buoyancy was equivalent to –0.77K temperature deviation and $0.024\ m\,s^{-2}$ downward acceleration in the momentum equation. The minimum temperature deviation was –1.38K at $z = 0.05km$, which gave $0.048\ m\,s^{-2}$ acceleration and was larger than the effect of the rain water loading as in the case in Run 1. If we estimate the values of $w^{\downarrow T}_{z=0}$ and $w^{\downarrow R}_{z=0}$ from the figure, they are $4.84\ m\,s^{-1}$ and $5.38\ m\,s^{-1}$ respectively, while the maximum values of these estimates in the region between $y = 15km$ and $y = 25km$ at $x = 27km$ during the period from $t = 265min$ to $t = 275min$ are $10.83\ m\,s^{-1}$ and $7.33\ m\,s^{-1}$, respectively, and the maximum estimate of $w^{\downarrow B}_{z=0}$ is $13.07\ m\,s^{-1}$, which is much less than the value of the gust speed of $18.0\ m\,s^{-1}$ realized in the model. The estimate of the gust speed must include the initial momentum which the air in the downdraught has in the upper levels.

In order to understand the process producing the surface gust, we examine the time change of the horizontal momentum budget at the grid point where the gust occurred (Fig. 10). The wind speed changed very quickly. The increase of the wind speed was very large from $t = 269min$ to $t = 273min$, i.e., $9\ m\,s^{-1}$ in 4 minutes. The wind speed attained its maximum value at $t = 273min$, when pressure rose 0.7hPa, temperature dropped 2K,

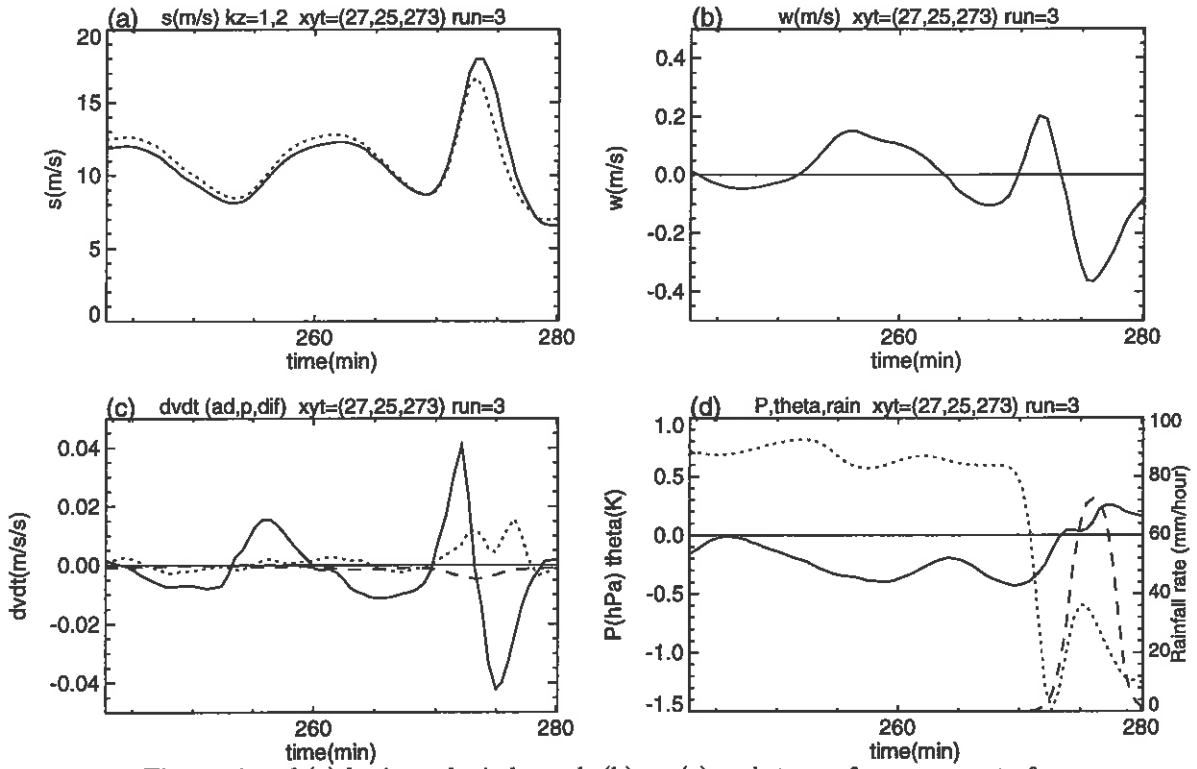

Figure 10: Time series of (a) horizontal wind-speed, (b) w, (c) each term of y-component of momentum equation, and (d) pressure, temperature deviation and rainfall at $x = 27km$, and $y = 25km$. The height is $z = 0.05km$, except for w at $z = 0.11km$ and dashed line in (a) at $z = 0.17km$. Solid line in (c) indicates the acceleration due to advection, dotted line the pressure gradient term, and dashed line the viscosity term. Solid line in (d) indicates the pressure deviation, dotted line the temperature deviation, and dashed line the rainfall rate.

and rain started to fall. This was also the time when the vertical motion changed sign from positive to negative. The period of upward motion before the maximum velocity corresponded to the period of horizontal convergence, i.e., to the period of acceleration due to horizontal advection, while the period of downward motion after the maximum velocity corresponded to the period of horizontal divergence, i.e., to the period of deceleration due to horizontal advection. In general, the effect of vertical advection was not so large as the effect of horizontal advection, and the sum of the two advection terms was positive in the convergence region with upward motion before the maximum velocity, and negative in the divergence region with downward motion after the maximum velocity (Fig. 10c). The effect of horizontal advection was important to the acceleration of the air. However, if we consider the growth of the peak gust with time following the point moving by the maximum wind velocity, the horizontal advection should be zero because of the zero derivative of the wind speed. The vertical advection decelerated the air at this maximum velocity point because the wind speed at the second level was smaller than the one at the first level as is shown in Fig. 10a, although it accelerate the lower layer air in general by the downward momentum transport. The diffusion term must be negative because the wind speed is the maximum in the surroundings. Therefore, the acceleration with time following the point must be due to the pressure gradient force. Fig. 10c shows that the pressure gradient force was positive and it made $\frac{dv}{dt}$ positive just before the wind velocity attained its maximum value and that it was necessary to grow the gust with time.

The importance of the pressure gradient force in the growth of horizontal wind velocity is revealed by studying the time change of the momentum budget along a parcel trajectory passing through the large gust (Fig. 11). The parcel was released from ($x = 20.0km$, $y = 8.5km$, $z = 1.5km$) at $t = 240min$. Fig. 12 shows the time changes of w, v, and the contributions of each term in equations (2) and (3) along the trajectory. The parcel descended slowly at first with increasing downward velocity to $1\,m\,s^{-1}$ at $t = 250min$, and came to the lowest level at $t = 273min$, and thereafter w was about zero. The downdraught was created mainly by the negative temperature deviation because the downdraught was located between active updraughts where the air was heated by condensation. The downward motion was decelerated by a strong upward directed pressure gradient force, which became larger as the parcel approached the surface and so stopped the downdraught.

The horizontal wind speed was decreased by the pressure gradient force when the parcel was descending. When the parcel came near to the surface, it was accelerated by the pressure gradient force, which gave 0.01 $m\,s^{-2}$ acceleration at maximum, enough large to increase the wind velocity from 8 $m\,s^{-1}$ to 18 $m\,s^{-1}$ in 20 minutes, shown in Fig. 10. Although the horizontal momentum in the downdraught was not conserved as is shown in Fig. 12b, it is not dissipated, but is decreased by the pressure gradient force. The horizontal momentum returns to its initial value when the air parcel is accelerated by the pressure gradient force as it exits from the high pressure region near the surface. So it is reasonable to include the initial horizontal momentum in the equation to estimate gust speed. If we assume that the initial kinetic energy of the air parcel in the downdraught is added the energy due to the work done by the buoyancy force, the equation estimating gust wind speed becomes

$$V_{gust} = \sqrt{\int_0^H -2g\left(\frac{\Delta\theta}{\Theta} - q_r\right) dz + v_{ini}(H)^2}, \tag{9}$$

where $v_{ini}(H)$ indicates the initial horizontal wind speed at z=H where the downdraught

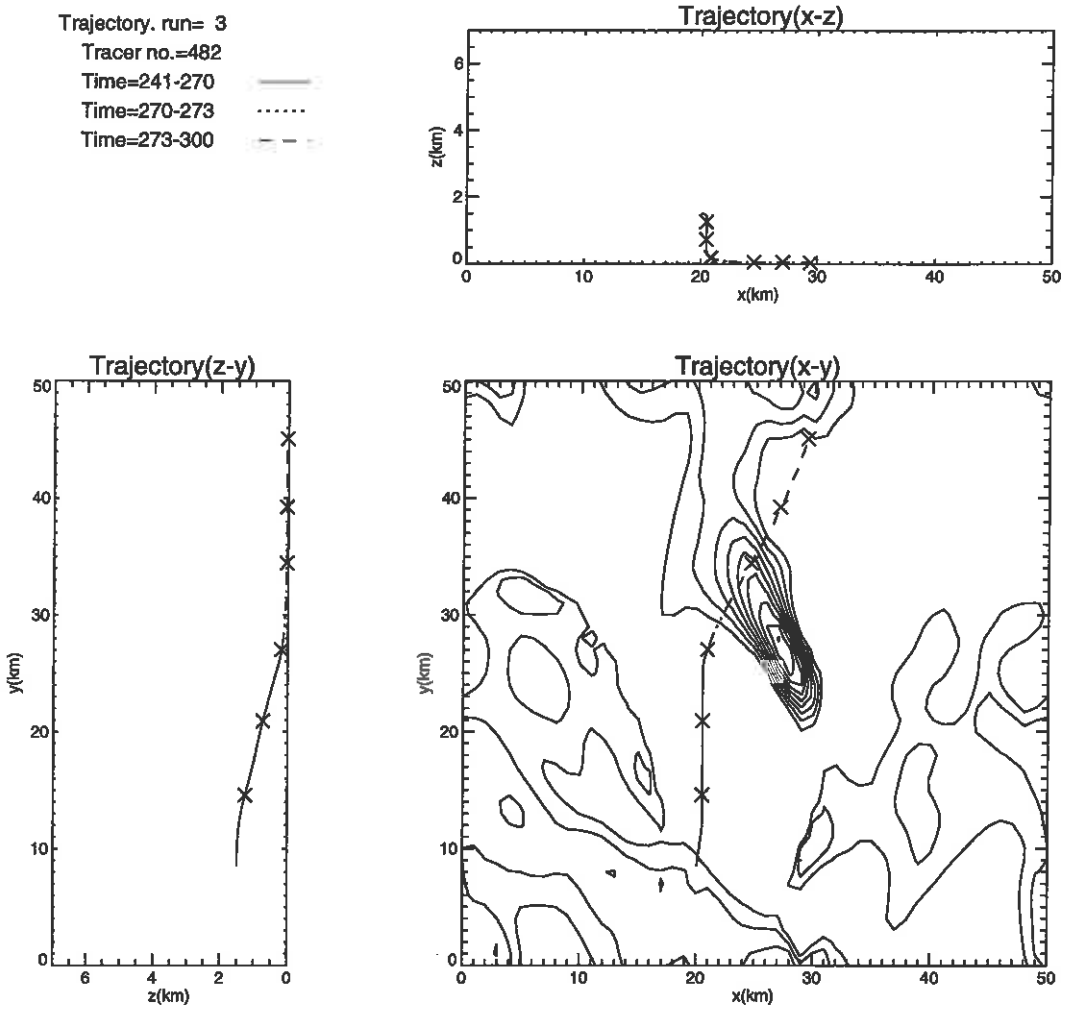

Figure 11: Trajectory of a parcel released from ($x=20.0km$, $y=8.5km$, $z=1.5km$) at $t=240min$. Solid lines indicate the trajectory between $t=240$ and $270min$, dotted lines indicate between $t=270$ and $273min$, and dashed lines indicate between $t=273$ and $300min$. Crosses indicate the position every 10 minutes. Contour lines in the x-y cross section are isopleths of horizontal wind speed at $z=0.05km$, $t=273min$. Contour interval is $1\,m\,s^{-1}$, and the minimum contour is $10\,m\,s^{-1}$.

starts. If we assume that the air parcel in the downdraught came from $z=2km$, i.e., if we assume the horizontal wind speed in the downdraught at its original level is $v_{ini}(H)$ =40 $m\,s^{-1}/6km \times 2km = 13.3\,m\,s^{-1}$, then V_{gust} is estimated as $18.65\,m\,s^{-1}$, which is as large as the gust speed realized in the model.

The temperature drop in strong downdraughts at the surface used in the Forecasters' Reference Book (1993) to estimate the gust speed is a good measure of the buoyancy force because the temperature drop is most significant at the surface as is shown in Fig. 5 and Fig. 9. The relationship between the peak gust and the temperature drop (Fawbush and Miller, 1954) can be used as an alternative presentation of the equation (6) without information of either rain mixing ratio or the original level of the downdraught. The maximum temperature drops at the lowest level in Runs 1 and 3 are about 2 K, and the

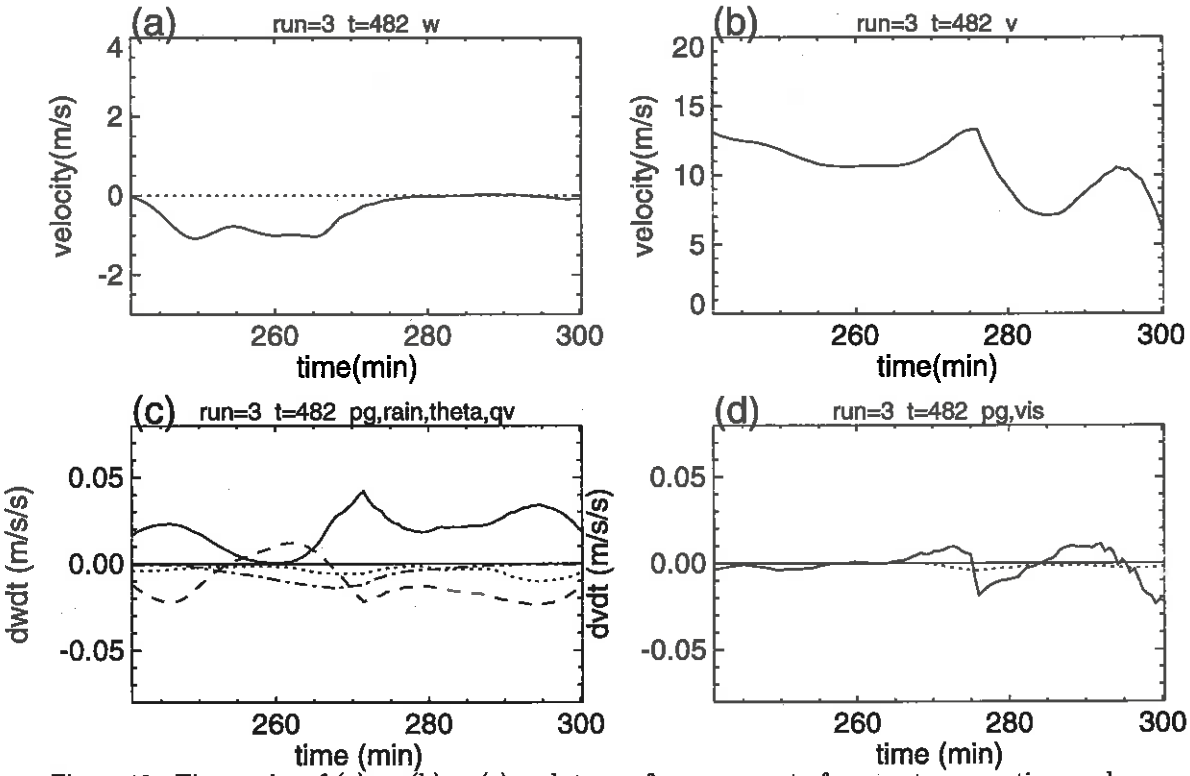

Figure 12: Time series of (a) w, (b) v, (c) each term of z-component of momentum equation, and (d) each term of y-component of momentum equation along the trajectory shown in Fig. 11. Solid lines in (c) and (d) indicate the acceleration due to the pressure gradient force, dotted line in (c) is rain loading term, dashed line temperature term, and dash-dotted line water vapour term. Dotted line in (d) indicates the viscosity term.

corresponding value of the peak gust from Fig. 1 in Fawbush and Miller (1954) is 10 $m\,s^{-1}$. Although the estimate is good for Run 1, it is too small for Run 3 because it does not include the initial wind effect sufficiently.

3.3. Equation for estimate of gust wind speed

Although the equation (9) in section 3.2 gives quite good estimates of the peak gusts, it is difficult to apply to the other occurrences of gusts in the experiments because too much data must be processes. Data which are readily available and potentially useful estimators are the maximum values of negative temperature deviation and rain water content over the model domain. These are the main terms driving downdraughts. Another important quantity is H, the level from where downdraughts started. It is required to evaluate the initial horizontal momentum of the air in downdraughts and to provide the upper limit of the integration of buoyancy force in downdraughts. In a numerical prediction model, the level H must be determined from the convective parameterization scheme. However, in this paper, we estimate H from the cloud-resolving model.

In order to estimate the original level of the air in downdraughts, we used a tracer whose density increases linearly with height, just like the horizontal wind in the initial field in Run 3. As the tracer is transported by convection we can estimate the initial level and hence the initial horizontal wind speed of the air in downdraughts from the value of the tracer in the downdraughts if it is well conserved. Although the eddy diffusivity of

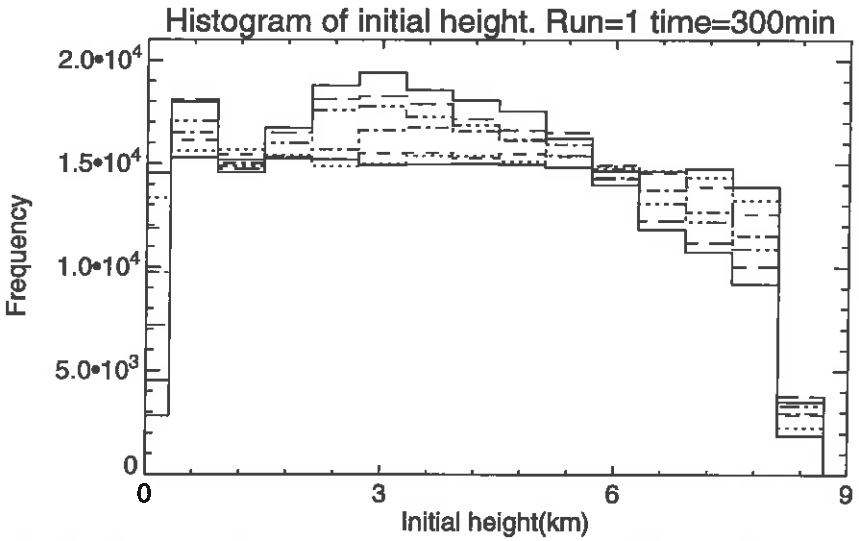

Figure 13: The histogram of the concentration of tracer at $t = 300min$. The x-axis is the corresponding height. Solid line almost constant at 15000 indicates the histogram of the tracer set at $t = 290min$, i.e. the histogram 10 minutes after setting. Dotted line, dashed line, dash-dotted line, dash-dot-dot-dot line, long dashed line, and another solid line indicate 20, 30, 40, 50, 60, and 70 minutes after setting, respectively. The data are interpolated to every 0.1 km in the vertical from $z = 0.05km$ to $z = 8.35km$ in order to avoid the effect of variable spacing of grid intervals. As the histogram is taken every 0.6 km and there are 50 × 50 grid points at one level, the frequency should be constant at 15000 at the setting time. The decrease of the frequency at $z = 8km$ is because only the data below $z = 8.35km$ were kept and used in the interpolation.

the tracer was set to be zero, it was mixed by numerical diffusion. Therefore, we entered new tracer every 10 minutes, and used the values of the tracers to which the effect of the numerical diffusion was small. Fig. 13 shows the histogram of the density of each tracer at $t = 300min$. It shows that the effect of the numerical diffusion was small in periods less than 30 minutes, which is long enough for convection to transport the air in downdraughts to the surface as is shown in Fig. 4 or Fig. 11. Therefore, we considered that the tracer concentration set within 30 minutes was conserved, and that the values in downdraughts indicate the original level of the air. The value we want to use as H is the value at the maximum horizontal wind speed at the lowest level. So the value at the maximum horizontal wind speed at each moment was kept and the maximum value within 30 minutes before the peak gust occurred is used as H in the following equations.

We estimated the gust speed from the buoyancy force using the equation of

$$V_{gust}^{B} = \alpha \sqrt{\int_0^H -2g \left(\frac{\Delta\theta_m}{\Theta} - q_{rm} \right) dz}. \tag{10}$$

where $\Delta\theta_m$ and q_{rm} are the maximum values of negative $\Delta\theta$ and q_r at each level. The maximum value of V_{gust}^{B} within 30 minutes before the peak gust occurred is used as the estimated gust speed. Fig. 14a shows the relation between the maximum gust speed in the numerical experiments of Runs 1, 2, and 3 and the estimated gust speed from the buoyancy force. The coefficient α is introduced because the maximum values of negative $\Delta\theta$ and q_r are likely to be overestimates of those occurring in downdraughts. The value of

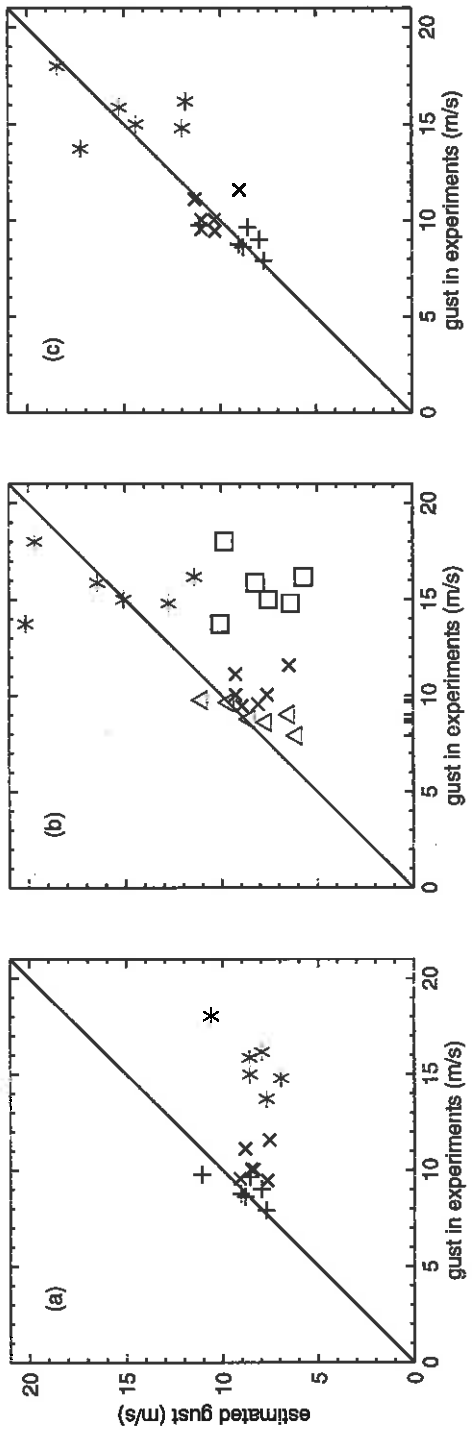

Figure 14: The relation between the gust speed in the numerical experiments and the gust speed estimated from (a) buoyancy force in the downdraught, (b) the original horizontal velocity of the air coming to the gust, and (c) the combination of the two mechanisms. Plus marks indicate results in Run 1, crosses in Run 2, and asterisks in Run 3. Triangles, crosses and squares in (b) indicate the level H in Runs 1, 2 and 3 if the vertical axis is replaced by a height axis with $6/\beta$ km corresponding to $20\,m\,s^{-1}$.

α used in the figure is 0.48, which is determined from the 6 results of Run 1, where only the buoyancy force is the origin of the gust speed. The estimate is too small for Runs 2 and 3 where vertical advection of initial wind plays an important role.

Fig. 14b shows the relation between the maximum gust speed and the estimated gust speed from the initial horizontal wind speed at H:

$$V_{gust}^{I} = \beta \, v_{ini}(H). \tag{11}$$

The coefficient β is 1.07, which is determined from the 12 results of Runs 2 and 3, where v_{ini} plays an important role in determining the gust speed. The estimate is much better for the large gust values of Runs 2 and 3 than equation (10). However, the estimates for the case with no initial wind (Run 1), as shown by pluses at the bottom of the figure, are of course very bad. Furthermore, the difference between Runs 2 and 3 is clear in the figure. There is a tendency for the estimates to be too small in Run 2 while they are too large in Run 3, if we use the common value for β in Run 2 and Run 3. This is because the effect of the buoyancy force is more important in Run 2, the small shear case, than in Run 3, the large shear case.

Fig. 14c shows the relation between the maximum gust speed and the gust speed estimated from the equation

$$V_{gust}^{B+I} = \alpha \sqrt{\int_0^H -2g \left(\frac{\Delta\theta_m}{\Theta} - q_{rm} \right) dz + \beta' \, v_{ini}(H)^2}, \tag{12}$$

i.e., the combination of the two mechanisms. The value of β' is 2.85 which is determined from all data of Runs 1, 2, and 3 using the value of $\alpha = 0.48$. The estimates do not show the tendency of small values in Run 2 and large values in Run 3, which is shown in Fig. 14b. The root mean square of the error in the estimates for the 12 cases in Runs 2 and 3 using equation (12) is $2.1 m\,s^{-1}$ which is smaller than $3.0 m\,s^{-1}$, the value using equation (11). The estimate using equation (12) is better than the other estimates showing that both mechanisms must be included in the equation to estimate the gust wind speed.

The crosses in Fig. 14b indicating V_{gust}^{I} in Run 2 also indicate the level H if the vertical axis is replaced by a height axis with $6/\beta$ km corresponding to 20m/s. The triangles and the squares indicate the results in Runs 1 and 3 on the same axis. These marks show the decreasing tendency of H with increasing shear which is consistent with the suppression of convection by shear. Although convections in Run 3 were organized in line structure and lasted longer than those in Run 1, it does not mean that the level H is higher in Run 3 than in Run 1. Furthermore, the long lifetime of the convection in Run 3 does not contribute to the large gust. The result is consistent with the result by Proctor (1989) that the strength of the gust does not depend on the duration of the downdraught if it lasted more than a few minutes.

4. Results with Coriolis force

4.1. Run 14 with Coriolis force and large geostrophic wind

The time series of the peak values in Run 14 with Coriolis force is shown in Fig. 15 in the same format as Fig. 2. The initial wind speed is $40 m\,s^{-1}$ which is equal to the

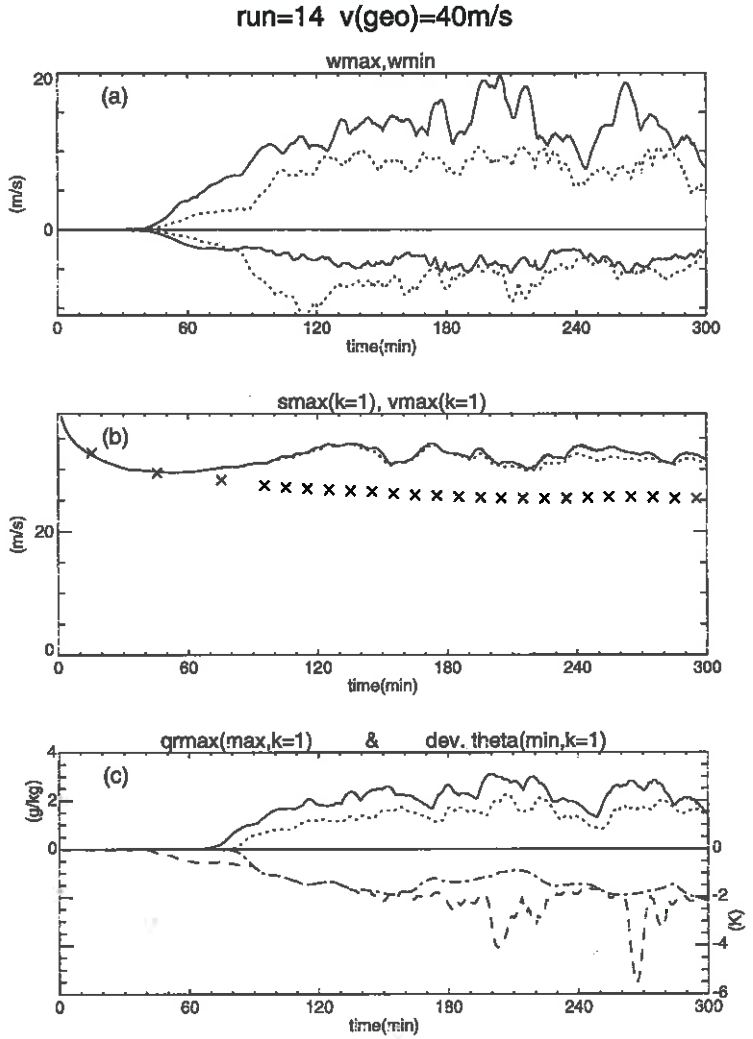

Figure 15: Time series of the peak values in Run 14 in the same format as in Fig. 2. Crosses in (b) indicate average y-component of velocity at the lowest grid level.

geostrophic wind and constant in the whole domain. The wind speed at level 1 decreased because of frictional retardation during the first 30 minutes, when there are no surface heat fluxes. Then the surface heat fluxes activated convection. The momentum flux became larger and the gust speed became larger although the average wind speed still decreased. The maximum gust speed occurring at $t=173min$ was $34.2\,m\,s^{-1}$, which was much larger than in Runs 1, 2 or 3 although the maximum updraught, temperature deviation and water content were smaller than the results in Run 1. This is because convection was suppressed by the shear which was created by the frictional retardation in the lower levels. We will use the six peak values at $t=125, 173, 195, 226, 242$ and $291min$ in order to derive an equation estimating gust speeds later in section 4.2, while we will discuss the peak gust at $t=242min$ in this section, because the convection pattern at this time was different from those in other Runs.

The horizontal cross section at the lowest level at $t=240min$, 2 minutes before the gust attained the peak value, is shown in Fig. 16a. The maximum horizontal wind speed

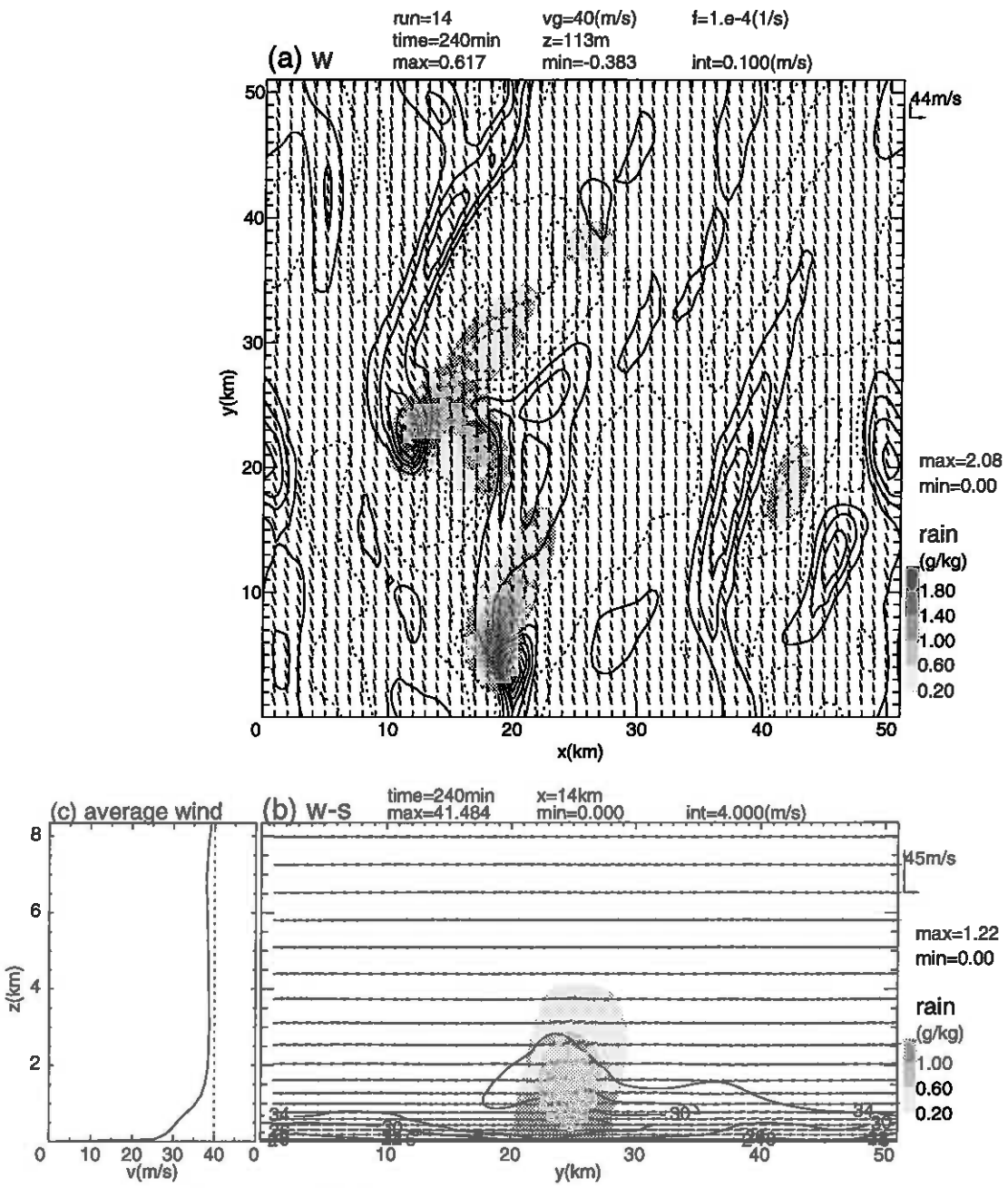

Figure 16: Horizontal and vertical cross sections and vertical profile of average wind speed as in Fig. 7 except for Run 14 at $t = 270min$, 3 minutes before the gust attained the maximum speed.

at the lowest level was 33.7 $m\,s^{-1}$, which occurs at ($x = 14km$, $y = 23km$) between the large upward motion at ($x = 12km$, $y = 22km$) and the maximum downward motion at ($x = 17km$, $y = 21km$). The average horizontal velocity at this level is (–5.26 $m\,s^{-1}$, 25.5 $m\,s^{-1}$). The negative u-component velocity was increasing with time, and the convective cells in the boundary layer tended to line up along the shear vector in good agreement with the linear theory of convection (e.g., Asai, 1970). The deviation from the geostrophic wind was very small in upper levels as is shown in Fig. 16b and c. The average value of the decrease of v was 4.8 $m\,s^{-1}$ at $z = 0.9km$, and decreased to 1.61 $m\,s^{-1}$ at $z = 1.9km$. It decreased slowly and remained about 1 $m\,s^{-1}$ to $z = 8km$ and then decreased rapidly

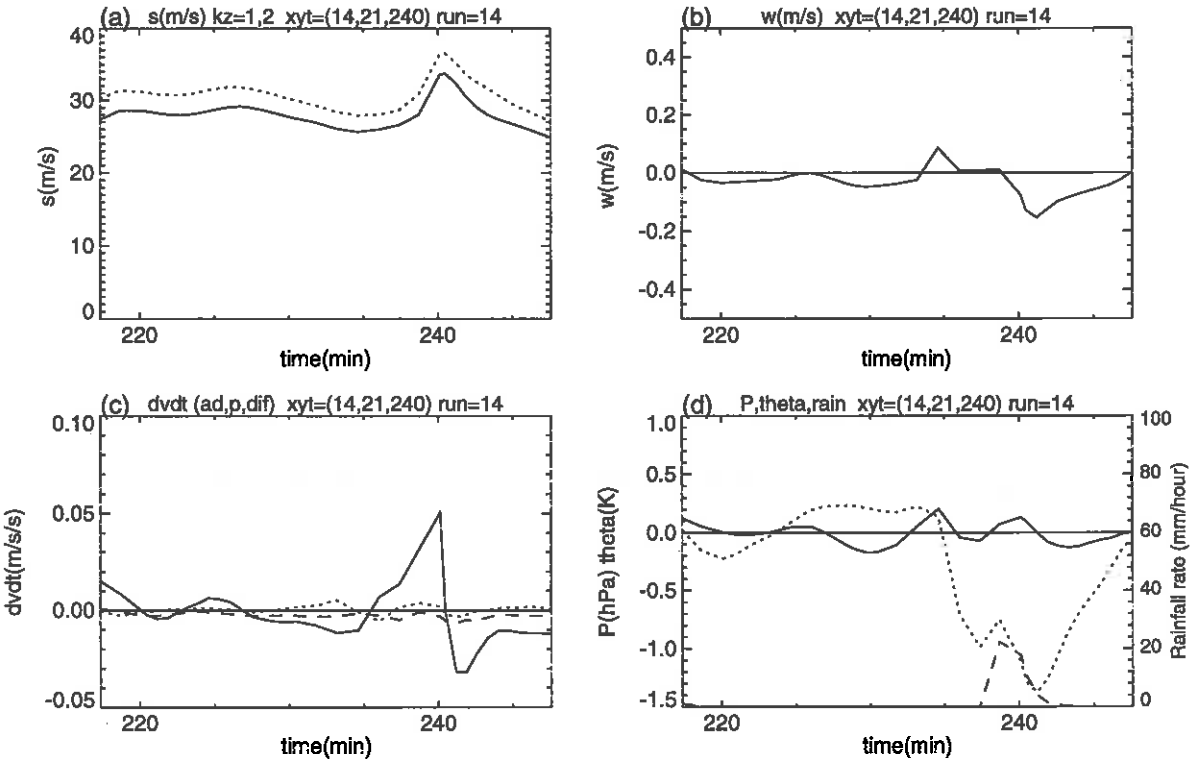

Figure 17: Time series of (a) horizontal wind-speed, (b) w, (c) each term of y-component of momentum equation, and (d) pressure, temperature deviation and rainfall at $x = 14km$ $y = 21km$, in the same format as in Fig. 10, but for Run 14.

at the top of the convective layer, about $z = 9km$. The decrease in wind speed extended to $z = 1km$ in the non convective region, but was confined to the lower levels in the downdraught region, i.e., air with higher wind speed was brought down to the lower levels by the downdraught. Furthermore, unlike in Fig. 7b, there were no maximum values at the lowest grid level.

Fig. 17 shows the time change of the horizontal momentum budget at $x = 14km$ $y = 21km$ $z = 0.05km$. The already strong wind became even stronger at about $t = 241min$ with a temperature drop of 1.5K and rainfall of $20mm\ hour^{-1}$. The effect of advection was the most important in the acceleration of the air. The pressure change was smaller than in Run 3, and its effect on the momentum budget was much smaller than the acceleration due to advection. The strong wind followed the strong wind at the upper level. The correlation between horizontal wind speed and vertical motion was –0.47 in this Run while it was –0.08 in Run 3. It also indicates the important role of vertical momentum transport in the gust generation in this Run.

4.2. Equation for estimate of gust wind speed

We will apply the equations (10), (11), and (12) of section 3.3 to the experiments with Coriolis force, which have constant geostrophic wind (Runs, 11, 12, 13, and 14), and experiments with geostrophic wind shear (Runs, 21, 22, 23, and 24). Fig. 18a shows the relation between the maximum gust speeds realized in the numerical experiments and the gust speeds estimated from the buoyancy force using equation (10). The coefficient α is

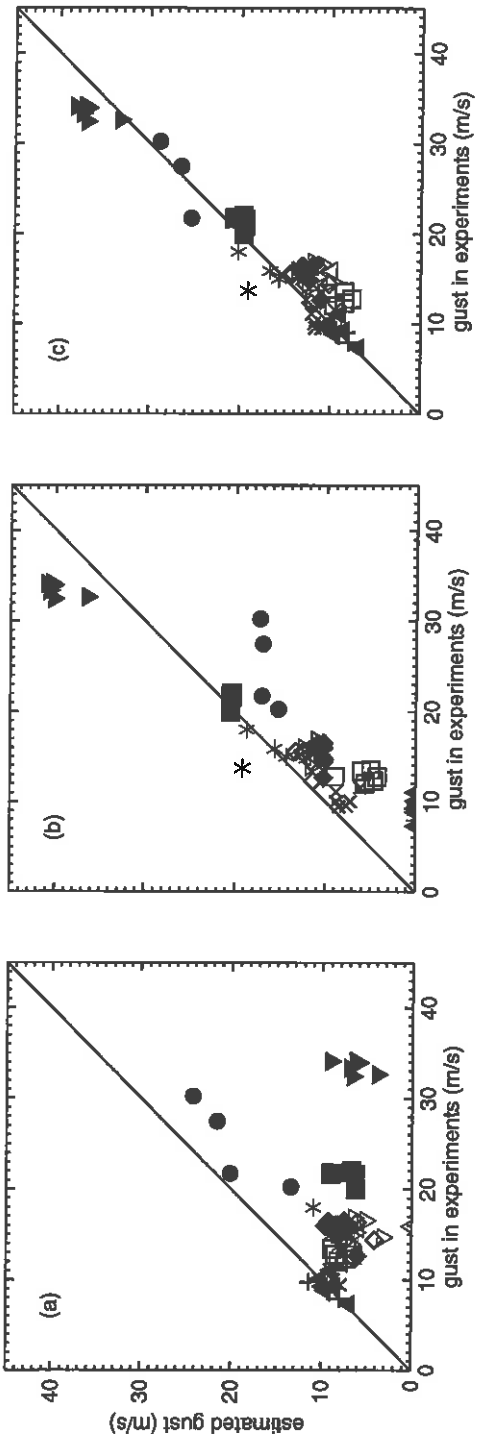

Figure 18: The relation between the gust speed in the numerical experiments and the estimated gust speed as in Fig. 14, but including the results for Runs 11, 12, 13, 14, 21, 22, 23, 24 and 31. Upward directed closed triangles indicate results in Run 11, closed diamonds, closed squares, and downward directed closed triangles indicate results in Run 12, 13 and 14, respectively, and upward directed open triangles, open diamonds, open squares, and downward directed open triangles indicate results in Run 21, 22, 23 and 24, respectively. Closed circles indicate the results in Run 31.

changed to 0.50, which is determined from the 12 results of Runs 1 and 11. As in Fig. 14a, the estimates are too small for the cases where the original wind speed plays an important role. The estimates even show negative correlation, i.e., the tendency of decrease with increasing the gust wind speed. This might be because convection is suppressed by the shear in the cases with high geostrophic winds. Fig. 18b shows the relationship between the maximum gust speed and the gust speed estimated from the initial horizontal wind using equation (11), in which $v_{ini}(H)$ is replaced by $\overline{|V(H)|}$, the horizontal mean value of horizontal wind speed at height H at each time of occurrence of the gust. The coefficient β is changed to 1.03, which is determined from the 54 results of Runs 2, 3, 12, 13, 14, 21, 22, 23, and 24 where initial wind fields play important roles in determining the gust speed. The estimate is much better for the large gust values than equation (10). However, it shows an over-estimate for strong gusts and under estimate for weaker gusts. This is because the effect of the buoyancy force is large in the weaker gusts as in Fig. 14b. Fig. 18c shows the relation between the maximum gust speed and the gust speed estimated from the combined effects using equation (12). The value of β' is 3.40 which is determined from all data of all Runs using the value of $\alpha = 0.50$. The estimate also shows a weak tendency that the estimates in Runs 12 and 13 are small and the estimates in Run 14 are large compared to the realized gust speeds. However, the error in the estimates is very small compared to other equations. The root mean square of the error in the estimates for the 54 cases using equation (12) is $3.12\, m\, s^{-1}$ which is much smaller than $4.67\, m\, s^{-1}$, the value using equation (11).

When the winds in the upper levels are strong, and there are no vigorous downdraughts or large surface heating, it can be assumed that the amount of turbulence depends on the mean wind and the 'roughness' of the surface, because the effects of buoyancy forces on the turbulence are negligible compared to the inertial forces. Then it can be assumed that gusts are caused solely by the vertical shear of the wind and the resistance of the rough ground, and that the geostrophic wind determined by the surface pressure is the main determining factor of the surface gust winds. In fact, experiment and theory confirm that maximum gusts should be estimated by the formula:

$$V_{gust} = \lambda V_{grad} \tag{13}$$

where V_{grad} is the mean wind immediately above the boundary layer, which is approximated by the geostrophic wind given by the large-scale surface pressure pattern, and λ lies in the range $0.5 - 0.9$, increasing with decreasing roughness. For the roughness length of the experiments λ is approximately 0.7. This calculation is well-founded in the literature on shear-driven turbulence, Panofsky and Dutton (1984). If we applied the equation (13) to the Runs, the value of λ is 0.835, higher than the value of 0.7, even in Run 14. The values for other Runs are larger than 1.0. The gust speeds exceeded the geostrophic wind speed which can not be explained by the transport of the initial momentum to downward. The pressure gradient force due to the buoyancy force plays an important role in the horizontal momentum budget in these Runs, although it is less important in Run 14. Formula (13) should not be used in convective situations, because it does not include the effect of the buoyancy force. On the other hand, the equation (12) can be used in wider ranges of circumstances because it includes both processes, momentum transport and buoyancy.

4.3. Run 31: An application to a thunderstorm case

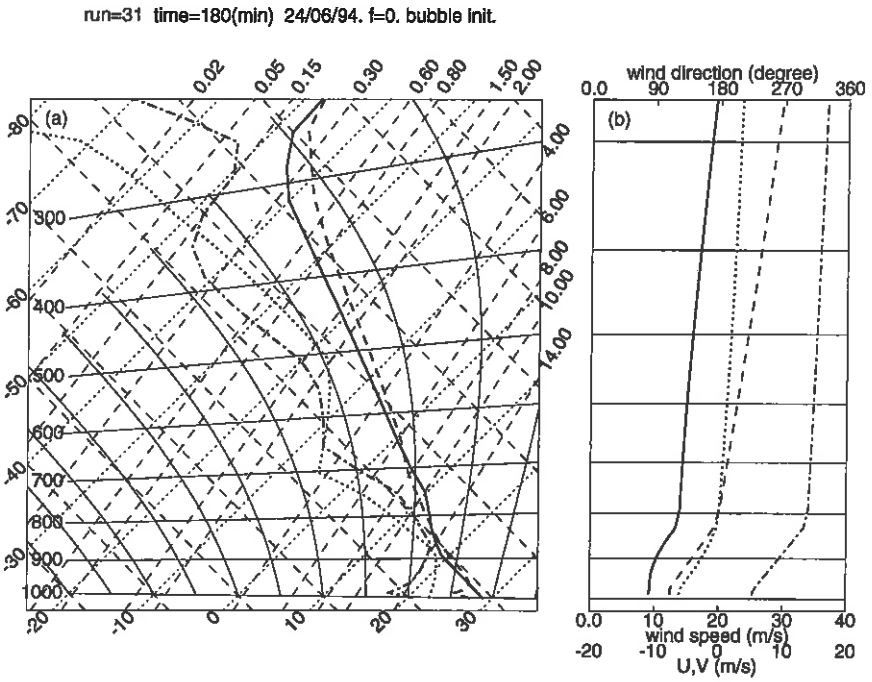

Figure 19: Vertical profiles of (a) temperature and dew point temperature and (b) wind speed and direction in Run 31. In (a), the thick solid line and and the thick dashed line indicate temperature and dew point temperature at $t = 0$. The dashed line and dash-dotted line indicate temperature and dew point temperature at $t = 180min$. In (b), the solid line indicates the wind speed and the dotted line indicates the wind direction, the dashed line and dash-dotted line indicate u and v, respectively.

The model and the estimation equations were applied to a thunderstorm case of 24th of June 1994, when gusts of up to $27 m\,s^{-1}$ were observed in a severe thunderstorm over South Eastern England. Fig. 19 shows the initial vertical profiles of temperature, dew point and wind which were extracted from analyses of the Meteorological Office Limited Area Model for the north coast of France (48.5°N, 2°W) at 1200 GMT. In the analyzed profile there was a strong stable layer between $z = 1km$ and $2km$ and active convection would not develop unless there was large-scale forcing such as horizontal convergence or differential advection. We assumed a mean vertical motion between $z = 0km$ and $3km$ whose maximum value was $5\,cm\,s^{-1}$ at $z = 1.5km$. The vertical profiles shown in Fig. 19 were the ones modified by the vertical motion for 1 hour. The vertical motion was continued for 30 minutes and then stopped. The wind speed was $10 m\,s^{-1}$ at the lowest level, increased to its maximum value of $22\,m\,s^{-1}$ at $z = 12km$ and decreased to $15\,m\,s^{-1}$ at the top of the domain. The direction of the wind changed from south-east at the surface to south-south-west above the boundary layer.

The time series of the peak values in Run 31 are shown in Fig. 20 in the same format as Fig. 2. The first convection developed to $t = 50min$, then it began to dissipate. The next convection which started to develop at that time could be maintained for more than 3 hours because the downdraught-induced gustfront interacted with the low-level environmental wind to produce the convergence necessary to sustain the convection.

The maximum gust speed at the lowest level ($32.6\,m\,s^{-1}$) occurred at $t = 210min$,

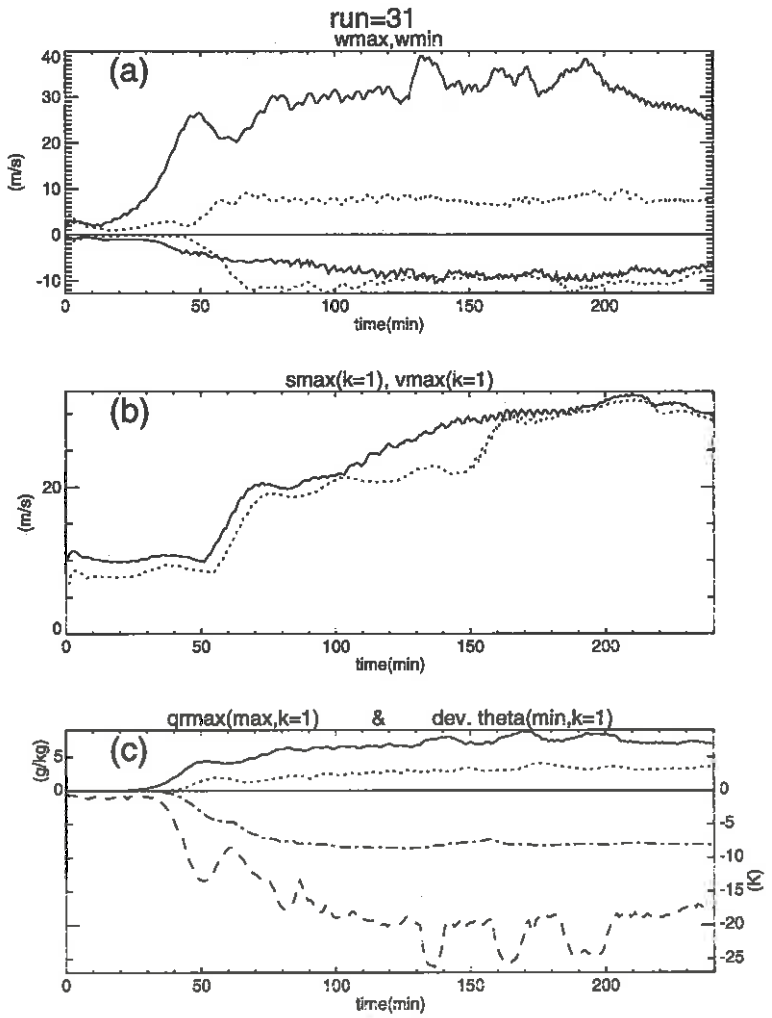

Figure 20: Time series of the peak values in Run 31 in the same format as in Fig. 2.

which is a little larger than the observed gust of $27 m\,s^{-1}$ on the southern coast of England at 1900 GMT. If we use the peak values at $t = 137, 166, 210$ and $226 min$ and apply the estimate equations for these occurrences of gust using the values of α, β and β' determined in section 4.2, we get the results marked by closed circles in Fig. 18. The results show that the estimate from the buoyancy force, i.e., equation (10) was better than the estimate from the initial wind, i.e., equation (11). This is because the effect of the buoyancy force was so large that the effect of the initial wind was not so important in the estimate. However, the estimate from the combined effects, i.e., equation (12), was the best of the three estimates in this case, confirming that both processes are important. The maximum temperature drop at the lowest level is 8.6 K, and the corresponding estimate of the peak gust from Fawbush and Miller (1954)'s method is $25 m\,s^{-1}$ which is not as good as equation (12). This is presumably because it does not take enough account of the initial horizontal momentum of the downdraught air.

5. Concluding remarks

Several numerical experiments have been performed using a cloud-resolving model to investigate the processes producing surface gusts under deep convection. The experiments confirm that the gusts are produced by two different processes, i.e., the distortion of downdraughts as they interact with the surface and the downward transport of horizontal momentum from upper levels. The relative importance of the two processes depends on the large-scale parameters such as vertical shear of the basic wind speed, geostrophic wind, and surface heat fluxes. The pressure gradient force produced by the downdraught is important even in the case of very large wind shear.

A parameterization equation for the gust speed must include both mechanisms to be useful in a wide range of external parameters. For all of the cases which we have studied, the gust speed is well estimated by the equation

$$V_{gust}^{B+I} = \alpha \sqrt{\int_0^H -2g \left(\frac{\Delta\theta_m}{\Theta} - q_{rm} \right) dz + \beta' \overline{|V(H)|}^2}, \tag{14}$$

which is an extension of the Fawbush-Miller formula, $V_{gust} = \sqrt{2(\frac{\Delta\theta}{\Theta})gH}$, to include the environmental wind speeds at higher levels, where $\Delta\theta$ is the anomaly of potential temperature from the horizontal average, Θ is the horizontal average of potential temperature, q_r is the rain mixing ratio, and H is the height of the level of origin of downdraughts. The coefficients determined from the results of the numerical experiments are $\alpha = 0.50$ and $\beta' = 3.05$. If the energy argument held exactly, and if our estimates of $\Delta\theta$ and q_r were exact, we would expect the values of α and β' to be 1.0. Note that $\alpha\sqrt{\beta'} = 0.87$, so only a small fraction of the initial transverse kinetic energy of the downdraught is dissipated by turbulence. The small value of α obtained indicates that the maximum values of $\Delta\theta$ and q_r are overestimates of the correct values for the modelled gusts. The more accurate analysis which we performed in sections 3.1 and 3.2 shows that values of $\alpha \approx 1.0$ and $\beta' \approx 1.0$ are appropriate if the correct values of $\Delta\theta, q_r$ and H can be obtained.

We have shown that, if we can estimate the values of $\Delta\theta, q_r$ and H, equation (14) can be used to estimate the strength of gusts in a variety of convective regimes. The next stage of this research will be to apply the equation in a numerical weather prediction model. In this case, $\Delta\theta, q_r$ and H, must be determined from the NWP model's convective parameterization scheme, and the values of α and β' must be determined empirically. This should enable the automatic prediction of gusts to be made in all convective situations, and it opens up the possibility of including an important boundary layer/convection interaction: the enhancement of surface fluxes due to subgrid-scale gustiness of the wind.

Acknowledgement

The authors would like to thank Prof. Keith Browning, Phil Brown, Dr. Imtiaz Dharssi, and Hugh Swann at the Joint Centre for Mesoscale Meteorology, and Prof. J.C.R.Hunt at Meteorological Office for their useful comments and discussions in this work. The numerical experiments were made on the Cray C90 at Meteorological Office whilst Dr. Nakamura was a visiting scientist at JCMM.

References

Asai, T., 1970: Three-dimensional features of thermal convection in a plane Couette flow. *J. Meteor. Soc. Japan*, **48**, 18–29.

Blackall, R. M., Brown, R., and C.G.Collier, 1990: Real-time analysis of surface wind gusts using radar data: 25th January 1990. *Met. Mag.*, **119**, 121–125.

Bond, J. E., Browning, K. A., and Collier, C. G., 1981: Estimates of surface gust speeds using radar observations of showers. *Met. Mag.*, **110**, 29–40.

Bradbury, W. M. S. and Deaves, D. M., 1994: The dependence of gust factor probabilities on convective activity: analysis conducted for Eurotunnel. *Meteorological Applications*, **1**, 159–164.

Bradbury, W. M. S., Deaves, D. M., Hunt, J. C. R., Kershaw, R., Nakamura, K., and Hardman, M. E., 1994: The importance of convective gusts. *Meteorological Applications*, 1, 365–378.

Browning, K. A., 1964: Airflow and precipitation trajectories within severe local storms which travel to the right of the winds. *J. Atmos. Sci.*, **21**, 634–639.

Collier, C. G., Dixon, J., Harrison, M. S. J., Hunt, J. C. R., Mitchell, J. F. B., and Richardson, D. S., 1994: Extreme surface winds in mid-latitude storms: forecasting and changes in climatology. *Journal of Wind Engineering and Industrial Aerodynamics*, **52**, 1–27.

Fawbush, E. J. and Miller, R. C., 1954: The types of airmasses in which North American Tornadoes form. *Bull. American Met. Soc.*, **35**, 154–165.

Forecasters' Reference Book, 1993: *Forecasters' Reference Book. Second edition.* Meteorological Office.

Fujita, T. T. and Caracena, F., 1977: An analysis of three weather-related aircraft accidents. *Bull. American Met. Soc.*, **58**, 1164–1181.

Klemp, J. B. and Wilhelmson, R. B., 1978: Simulations of right- and left-moving storms produced through storm splitting. *J. Atmos. Sci.*, **35**, 1097–1110.

Knupp, K. R., 1989: Numerical simulation of low-level downdraft initiation within precipitating cumulonimbi: Some preliminary results. *Mon. Wea. Rev.*, **117**, 1517–1529.

Panofsky, H. A. and Dutton, J. A., 1984: *Atmospheric turbulence. Models and methods for engineering applications*, 129 and 159–161. John Wiley, New York.

Parsons, D. B. and Weisman, M. L., 1993: A numerical study of a rotating downburst. *J. Atmos. Sci.*, **50**, 2369–2385.

Proctor, F. H., 1988: Numerical simulation of an isolated microburst. Part I: Dynamics and structure. *J. Atmos. Sci.*, **45**, 3137–3160.

Proctor, F. H., 1989: Numerical simulation of an isolated microburst. Part II: Sensitivity experiments. *J. Atmos. Sci.*, **46**, 2143–2165.

Shutts, G. J. and Gray, M. E. B., 1994: A numerical modelling study of the geostrophic adjustment process following deep convection. *Quarterly Journal of the Royal Meteorological Society*, **120**, 1145–1178.

Straka, J. M. and Anderson, J. R., 1993: Numerical simulations of microburst-produsing storms: some results from storms observed during COHMEX. *J. Atmos. Sci.*, **50**, 1329–1348.

CURRENT JCMM INTERNAL REPORTS

This series of JCMM Internal Reports, initiated in 1993, contains unpublished reports and also versions of articles submitted for publication. The complete set of Internal Reports is available from the National Meteorology Library on loan, if required.

1. **Research Strategy and Programme.**
   K A Browning et al
   January 1993

2. **The GEWEX Cloud System Study (GCSS).**
   GEWEX Cloud System Science Team
   January 1993

3. **Evolution of a mesoscale upper tropospheric vorticity maximum and comma cloud from a cloud-free two-dimensional potential vorticity anomaly.**
   K A Browning
   January 1993

4. **The Global Energy and Water Cycle**
   K A Browning
   July 1993

5. **Structure of a midlatitude cyclone before occlusion.**
   K A Browning and N Roberts
   July 1993

6. **Developments in Systems and Tools for Weather Forecasting.**
   K A Browning and G Szejwach
   July 1993

7. **Diagnostic study of a narrow cold frontal rainband and severe winds associated with a stratospheric intrusion.**
   K A Browning and R Reynolds
   August 1993

8. **Survey of perceived priority issues in the parametrizations of cloud-related processes in GCMs.**
   K A Browning
   September 1993

9. **The Effect of Rain on Longwave Radiation.**
   I Dharssi
   September 1993

10. **Cloud Microphysical Processes - A Description of the Parametrization used in the Large Eddy Model.**
H Swann
July 1994

11. **An Appreciation of the Meteorological Research of Ernst Kleinschmidt.**
A J Thorpe
May 1992

12. **Potential Vorticity of Flow Along the Alps.**
A J Thorpe, H Volkert and Dietrich Heimann
August 1992

13. **The Representation of Fronts.**
A J Thorpe
January 1993

14. **A Parametrization Scheme for Symmetric Instability: Tests for an Idealised Flow.**
C S Chan and A J Thorpe
February 1993

15. **The Fronts 92 Experiment: a Quicklook Atlas.**
Edited by T D Hewson
November 1993

16. **Frontal wave stability during moist deformation frontogenesis. Part 1. Linear wave dynamics**
C H Bishop and A J Thorpe
May 1993

17. **Frontal wave stability during moist deformation frontogenesis. Part 2. The suppression of non-linear wave development.**
C H Bishop and A J Thorpe
May 1993

18. **Gravity waves in sheared ducts.**
S Monserrat and A J Thorpe
October 1993

19. **Potential Vorticity and the Electrostatics Analogy: Quasi-Geostrophic Theory.**
C Bishop and A J Thorpe
November 1993

20. **Recent Advances in the Measurement of Precipitation by Radar.**
A J Illingworth
April 1993

21. **Micro-Physique et Givrage. Cloud Microphysics and Aircraft Icing.**
A J Illingworth
May 1993

22. **Differential Phase Measurements of Precipitation.**
M Blackman and A J Illingworth
May 1993

23. **Estimation of Effective Radius of Cloud Particles from the Radar Reflectivity.**
N I Fox and A J Illingworth
May 1993

24. **A Simple Method of Dopplerising a Pulsed Magnetron Radar.**
L Hua, A J Illingworth and J Eastment
November 1993

25. **Radiation and Polar Lows.**
George C Craig
February 1994

26. **Collected preprints submitted to International Symposium on the Life Cycles of Extratropical Cyclones; Bergen, Norway, 27 June - 1 July 1994**
April 1994

27. **Convective Frontogenesis**
Douglas J Parker and Alan J Thorpe
April 1994

28. **Improved Measurement Of The Ice Water Content In Cirrus Using A Total Water Evaporator**
Philip R A Brown and Peter N Francis
April 1994

29. **Mesoscale Effects of a Dry Intrusion within a Vigorous Cyclone**
K A Browning and B W Golding
April 1994

30. **GEWEX Cloud System Study, Science Plan**
May 1994

31. **Parametrization of Momentum Transport by Convectively Generated Gravity Waves**
R Kershaw
February 1995

32. **Mesoscale Modelling Newsletter, No. 5**
May 1994

33. **Observations of the mesoscale sub-structure in the cold air of a developing frontal cyclone**
K A Browning, S A Clough, C S A Davitt, N M Roberts and T D Hewson
May 1994

34. **Longwave Radiative Forcing of a Simulated Tropical Squall Line**
Imtiaz Dharssi
July 1994

35. **On the nature of the convective circulations at a kata-cold front**
K A Browning
September 1994

36. **Collected preprints of papers submitted to the COST-75 International Seminar on Advanced Weather Radar Systems, Brussels, 20-23 September 1994**
November 1994

37. **Use of satellite imagery to diagnose events leading to frontal thunderstorms: Parts I and II of a case study**
K A Browning and N M Roberts
November 1994

38. **The role of spaceborne millimetre-wave radar in the global monitoring of ice cloud**
P R A Brown, A J Illingworth, A J Heymsfield, G M McFarquhar, K A Browning and M Gosset
December 1994

39. **Potential Vorticity Inversion**
Michal Ziemianski
October 1994

40. **Theory of mature tropical cyclones; A comparison between Kleinschmidt (1951) and Emanual (1986)**
Suzanne L Gray
December 1994

41. **Dispersion and removal of pollutants during the passage of an atmospheric frontal system**
N R Gimson
December 1994

42. **The role of snow sublimation in frontogenesis**
D J Parker and A J Thorpe
December 1994

43. **Potential vorticity and the electrostatics Analogy: Ertel-Rossby formulation**
A J Thorpe and C H Bishop
December 1994

44. **Mesoscale aspects of extratropical cyclones: an observational perspective**
K A Browning
January 1995

45. **A Polar Low Outbreak: Evolution and Mesoscale Structures**
T D Hewson, G C Craig and C Claud
February 1995

46. **Generation of near-surface gusts by deep convection**
K Nakamura and R Kershaw
April 1995

Met Office Joint Centre for Mesoscale Meteorology Department of Meteorology
University of Reading PO Box 243 Reading RG6 6BB United Kingdom
Tel: +44 (0)118 931 8425 Fax: +44 (0)118 931 8791
www.metoffice.com